Characterization and Biomimetic Fabrication Study of Fetal Membranes for Understanding and Prevention of Preterm Birth

by Mackenzie L. Wheeler, M.S.B.E.

May 2022

Directed by: Teresa J. Ryan, Ph.D.

Department of Engineering

Preterm birth is defined as a baby being born before 37 weeks gestation and is a large problem, affecting 10% of all pregnancies in the United States and world annually. Preterm birth can result in lifelong complications for the infant or even death, considering the fetus continues developing vital organs throughout the last few weeks of pregnancy. Over the course of pregnancy, several layers and sub-layers are formed in order to protect the fetus from the external environment. Two of the most crucial layers that were heavily focused on throughout this project were the amnion and the chorion layers, which combine to make the placental membrane that surrounds the fetus. Preterm birth most often occurs due to mechanical failure of the membranes. Collagen proteins make up the strength and elasticity of the fetal membranes, supporting the fetus. If these proteins fail, this increases the chance of preterm birth occurring. A degrading enzyme, known as collagenase, often affects the membranes through bacteria and infections, breaking down the collagen fibers and leading to premature rupture of membranes or preterm pre-labor rupture of membranes. To study this process, a few different routes were taken. Artificial gels were tested on a nanoindentation machine to gather preliminary data to compare nanoindentation on real tissue. Artificial biomimetic membranes were also electrospun and mechanically tested on a macroscale. The goal of the biomimetic electrospun fiber mat is to be used to patch the woman's rupture site

after pre-labor rupture of membranes occurs. Four different mat categories were fabricated: not treated crosslinked (NX), not treated uncrosslinked (NU), treated crosslinked (TX), and treated uncrosslinked (TU). Treatment indicates that they were placed in the oven. Human fetal membranes were also mechanically tested on a macroscale after being submerged and incubated at two different set times in a control solution and varying levels of collagenase concentrations, including 45 U/mL and 135 U/mL. Fourier transform infrared spectroscopy of natural tissues was then used to analyze the integrity of the collagen molecules.

The results for this study indicate that through nanoindentation, the elastic modulus of two different types of hydrogels were consistently lower than anticipated. In regard to electrospinning, the uncrosslinked fiber mats have significantly greater strength than the crosslinked fiber mats. The fetal membrane results showed that overall, there was significant decrease in elastic modulus when membranes were submerged in a high collagenase concentration. Strength of the fetal membranes decreased significantly as collagenase concentration and incubation time increased. These findings suggest that collagenase buildup within the human body can potentially lead to preterm birth.

Overall, this work sought to study the biomechanical properties of fetal membranes. In current literature, there have been strength and elastic modulus values of placental membranes obtained through different modes of testing, but never through biaxial puncture testing. This project focused on a new approach of mechanically testing placental membranes.

Characterization and Biomimetic Fabrication Study of Fetal Membranes for Understanding and Prevention of Preterm Birth

A THESIS

Presented to the Faculty of the Department of Engineering

College of Engineering and Technology

East Carolina University

In Partial Fulfillment of the Requirements For the Degree

Master of Science in Biomedical Engineering

by

Mackenzie L. Wheeler

May, 2022

Characterization and Biomimetic Fabrication Study of Fetal Membranes for Understanding and Prevention of Preterm Birth

By

Mackenzie L. Wheeler

APPROVED BY:

DIRECTOR OF
THESIS: _____

Teresa J. Ryan, Ph.D.

COMMITTEE MEMBER: _____

Linda E. May, Ph.D.

COMMITTEE MEMBER: _____

Shanyue Guan, Ph.D.

CHAIR OF THE
DEPARTMENT OF ENGINEERING: _____

Barbara J. Muller-Borer, Ph.D.

DEAN OF THE
GRADUATE SCHOOL: _____

Paul J. Gemperline, Ph.D.

ACKNOWLEDGMENTS

This work has primarily been supported by ECU's Division of Research Economic Development and Engagement, the College of Engineering and Technology, and the Engineering Department. I have also been supported by the ECU graduate school, The Undergraduate Research and Creativity Activity Award, and the Research Mini Award. Thank you to the Engineering Department for five years worth of learning, growing, memories and lifelong friendships with students and faculty.

I would like to thank Dr. Michelle Oyen for being a pivotal support throughout the duration of my undergraduate and graduate research, and for encouraging me to pursue a master's degree in biomedical engineering. Dr. Oyen's support and advice has pushed me mentally and academically to overcome many obstacles and I am very grateful. I would also like to acknowledge my thesis committee chair, Dr. Teresa Ryan, for always being a quick response to my endless questions and providing guidance. Thank you to Dr. Linda May and Dr. Shanyue Guan for being a part of my thesis committee and providing expert knowledge on pregnancy and mechanics of materials. Thank you, Dr. Hui Bian, for helping me complete the statistical analysis of my project. Thank you to the girls at Columbia University, Dr. Kristin Myers, Daniella Fodera, and Nicole Lee, for collaborating with me on the nanoindentation project. Also, a huge thank you is due to my fellow student researchers and classmates, including Thomas Buckner, Maycie McDougal, Jeremiah James, Lucci DeRose, Mohammad Islam, Joey Hampton, and Branson Rogers for the long hours in the lab and pushing me on the difficult days.

Beyond the support at ECU, a huge thanks is due to my family and friends for their prayers over the last five years. Thank you to my mom, dad, grandparents, and siblings for always reminding me of what I'm capable of – anything I set my mind to. Thank you, Michael, for encouraging me every day to change the world.

TABLE OF CONTENTS

LIST OF TABLES

Table **Page**

LIST OF FIGURES

CHAPTER 1

INTRODUCTION

The definition of a full-term pregnancy is a pregnancy that lasts 37–40 weeks, which is important due to the fetus' brain and lungs continuing to develop throughout the last few weeks of gestation [1]. Preterm birth occurs often and is when the baby is born before 37 weeks [2]. Preterm birth is the leading cause of infant death and occurs 1 in 10 pregnancies nationwide and worldwide every year [3]. The earlier a baby is born, there is a greater risk of morbidity and mortality [4]. There is an increased chance the child has of health issues either as an infant or lifelong, such as respiratory disease, sepsis, intraventricular hemorrhage, and necrotizing enterocolitis, along with many other issues [4].

In addition to physical challenges that can arise from preterm birth, it can also serve as a heavy financial burden for many. When a baby is born preterm, the best option for them is to stay in the hospital's neonatal intensive care unit (NICU) to ensure they receive the utmost support from the nurses and physicians. Table 1.1 shows the average cost for a baby's NICU stay at different gestational ages.

Preterm birth can happen for a plethora of reasons, with preterm pre-labor rupture of membranes (PPROM) as one of the leading causes, affecting approximately one-third of preterm births [6]. Preterm pre-labor rupture of membranes occurs when the placental membranes are ruptured before 37 weeks gestation and before labor onset [6].

Preterm birth can be diagnosed at the woman's routine prenatal obstetrics check-ups. If she is experiencing regular contractions or advancing cervix dilation prior to 37 weeks gestation, then the woman will most likely be diagnosed with preterm labor [7]. Further testing is conducted to

Table 1.1: Average costs for NICU stays for preterm babies [5].

	Gestastional Age (Weeks)	**Average Length of Hospital Stay (Days)**	**Average Hospital Charges (Dollars)**
	All Admissions	13.2	76,164
	<32	46.2	280,811
	32-33	20.3	102,182
Preterm↑	34-36	9.8	51,083
	37-38	5.9	37,137
	39-41	4.9	29,771
	42+	6.5	47,282

differentiate this diagnosis. These tests include a pelvic exam, an ultrasound, uterine monitoring, and several lab tests [7]. Pelvic exams include the health care provider checking for placenta previa, uterine bleeding, and cervix dilation [7]. Ultrasound can also be utilized to check the size of the cervix, placental problems, the amount of amniotic fluid, and fetal weight and position [7]. Uterine monitoring includes the use of a monitor placed on the woman's abdomen to measure how long each contraction lasts and the time between each contraction [7]. Lastly, the health care provider can conduct a lab test by taking a sample of secretions from the woman's vagina to test for infections and fetal fibronectin, which essentially holds the amniotic sac and the uterus together [7], [8]. Figure 1.1 shows the development of a fetus throughout a pregnancy. It should be noted that critical parts of the body are still developing within the last few weeks of pregnancy, therefore, it is crucial that the fetus stay in utero until full-term ($\geq$ 37 weeks).

With this in mind, it is important to understand causes of PPROM, in order to treat and prevent its occurrence. Thus, this project studied one crucial concept suspected to be a factor in PPROM: collagenase enzyme buildup. Collagenase is a protein enzyme that forms if there is an infection. Collagenase degrades collagen fibers that provide fetal membranes with strength and elasticity. In order to verify or refute the impact of collagenase on fetal membrane mechanical properties, it is

critical to understand how much it alters the properties of placental membranes within a controlled experiment.

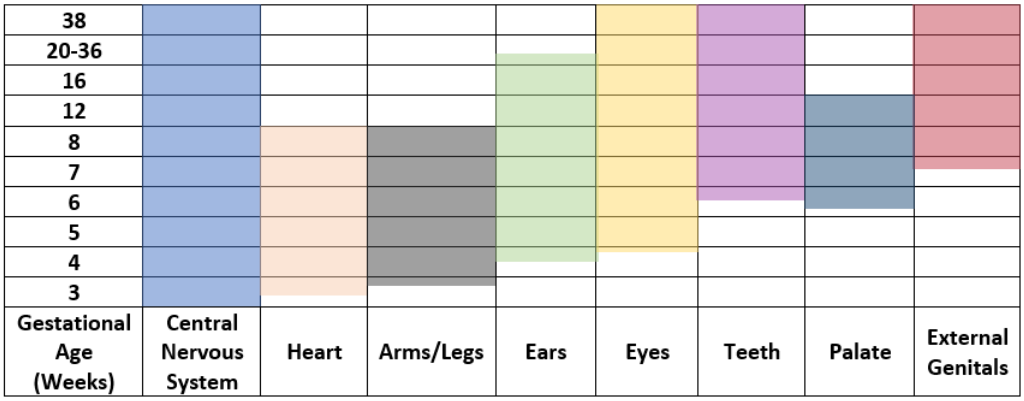

Figure 1.1: The development of a fetus throughout the course of pregnancy [9].

If a woman is diagnosed with preterm labor, various treatments can be completed in order to keep both the woman and child as safe and healthy as possible. Methods such as medications or surgical procedures can be used to treat this diagnosis [7]. Medications such as corticosteroids, magnesium sulfate, tocolytics, and progesterone hormone shots can be used to enhance the health of the child [7], [10]. Corticosteroids can be used to help the fetal lungs continue developing [7]. In addition to corticosteroids, tocolytics may be administered to slow contractions, thus delaying preterm labor, and allowing the corticosteroids to work to their full capacity [7]. Magnesium sulfate may be prescribed by the health care provider to lower the risk of cerebral palsy for the baby [7]. These medication remedies are suggested for women who are at risk of PPROM and between 24 and 34 weeks gestation [7]. For women that go into preterm labor due to cervical dilation, a surgical procedure referred to as a cervical cerclage is often completed. A cervical cerclage includes the health care provider stitching the cervix closed with sutures, similar to a drawstring bag being drawn shut. This surgical procedure is recommended when the fetus is less than 24 weeks gestation [7].

There are several cases of high risk pregnancies that increase the chance of a woman going into preterm labor or preterm birth. These include the woman previously having a preterm delivery, multifetal pregnancy, or having uterus or cervix incompetence currently or previously [3]. Although it is not always avoidable, there are several methods to prevent preterm labor and preterm birth. It is important that the woman achieve a healthy weight before becoming pregnant and ensure that they gain the appropriate amount of weight during pregnancy [3]. Smoking, drinking alcohol, and living with chronic health conditions can also increase the chance of preterm labor or preterm birth [3]. It is also of high importance that the woman visits a health care provider for a prenatal check-up as soon as they believe they are pregnant [3]. Making sure the woman's stress levels are reduced during pregnancy is crucial and can be more likely achieved by being active every day and consuming healthy foods [3]. Lastly, it is important for a woman to note that they should not try to become pregnant again until 18 months after their previous pregnancy [3].

Many of the current preventions of preterm labor and preterm birth include the way the woman lives, such as what she puts in her body, if she routinely sees her health care provider for prenatal check-ups, and how soon they become pregnant again after giving birth [3]. But, when asked the question "What are people doing to prevent preterm birth after the onset of preterm labor?" there are many limitations.

In addition to the reasons already mentioned as to how placental membranes can rupture, there are times when doctors pierce the membrane, such as for amniocentesis or when fetal surgery needs to be conducted. Therefore, the idea of artificial patches has been implemented for this project in the case where the placental membranes are intentionally or naturally ruptured. The idea is to have the doctor patch the woman's rupture site with this artificial biomimetic patch to allow the fetus more time in utero. This artificial patch is composed of biomimetic materials, such as gelatin.

Three primary steps were conducted for this study. The first part of this study focused on the nanoindentation testing of two hydrogels. The second part of this project focused on the creation of biomimetic membranes (two gelatin polymer solutions: uncrosslinked electrospun mats

and crosslinked electrospun mats) that can be used as a model system for research purposes and a potential patch to repair a placental rupture site in cases of preterm rupture of membranes. The third part of this project focused on the mechanics of real fetal membranes and analyzed the effects of varying concentrations of degrading enzymes, such as collagenase, on these membranes. Comprehending the negative effect these enzymes can have on the membranes is a crucial factor in understanding how placental membranes mechanically fail during pregnancy, leading to preterm rupture of membranes.

This chapter served as an introduction to this project focusing on the mechanical stiffness and strengths of fetal membranes. The second chapter provides a brief background of the anatomy of a pregnancy, including the layers that form during fetal development, the definition and explanation of preterm birth; discusses the mechanical properties found in the current literature of a woman's cervix and fetal membranes, and an introduction to biomimetic materials.

CHAPTER 2

ANATOMY AND BIOMIMETICS

2.1 Preterm Birth

Preterm birth can affect the baby in the short-term, such as organ complications due to them not being fully developed, or there can be lifelong complications such as cerebral palsy, impaired learning, and chronic health issues [11]. As can be seen in Figure 2.1, there are numerous specialized tissue layers that form during pregnancy of both fetal and maternal origin; it is crucial for maternal and fetal health that these tissue layers develop and work together properly. First, the amniotic fluid surrounds and cushions the fetus for protection [2]. The umbilical cord stems from the amniotic fluid and emanates from the placenta which delivers all the necessary oxygen and blood supply to the fetus. Next are the amnion and the chorion layers. These layers are often referred to as the chorioamnion (CA) membrane where the amnion is on fetus side and holds in the amniotic fluid [2]. Although the amnion is thinner than the chorion, it is stronger than the chorion [12]. Next is the decidua which helps detect what substances pass through the maternal membranes. The myometrium lays along the decidua as the muscular part of the uterus, with the uterine wall as the outermost layer furthest from the fetus [2].

As each of these layers are vital to the development of a healthy fetus, the layers that will be heavily emphasized in this project are the placental membranes, or CA. Interestingly, the placenta is the only temporary organ in the body and is highly dependent upon mechanical factors. Although there has been research conducted on this topic, there is still much to learn about the numerous factors that can trigger preterm birth.

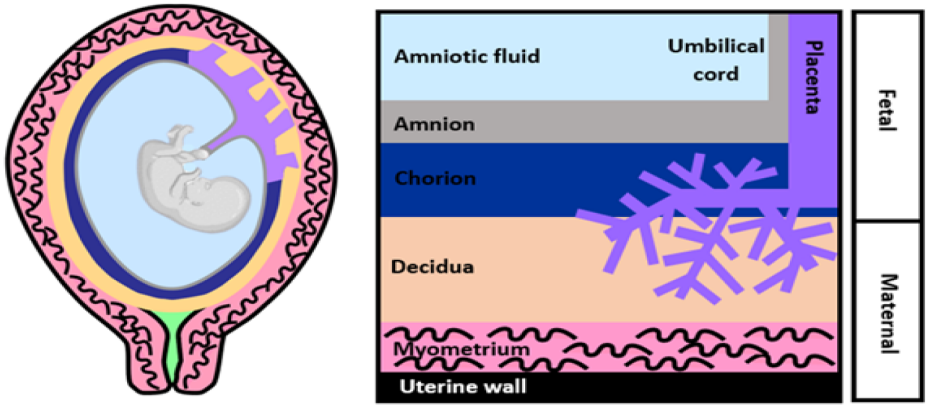

Figure 2.1: Color-coded development of essential layers of pregnancy, distinguishing maternal side and fetal side [13].

2.1.1 PPROM and Fetal Membranes

Pre-labor rupture of membranes (PROM) occurs when the fetal membranes rupture at full-term but before the onset of labor [6]. When this occurs, the amniotic fluid is released, which is what many people refer to as a woman's "water breaking." Preterm pre-labor rupture of membranes (PPROM) is the most devasting category of membrane rupture as it can cause the most significant damage to the health of the fetus and even the woman [6]. Preterm pre-labor rupture of membranes increases maternal and fetal risk of morbidity and mortality [6]. As mechanical factors play a large role in the rupture of membranes, prior to and at full term, cervical insufficiency is one of the most researched causes involving PROM and PPROM.

The fetal membranes are composed of the chorion and amnion membranes which merge during pregnancy to form the chorioamnion (CA) [14]. Another layer, referred to as the maternal decidua, is connected to the fetal membranes at the chorion. The CA and maternal decidual layers together surround the fetus during development, acts as a barrier from the external environment, and are known as the placental barrier. Figure 2.2 shows a micrograph of the fetal membrane and decidual layers.

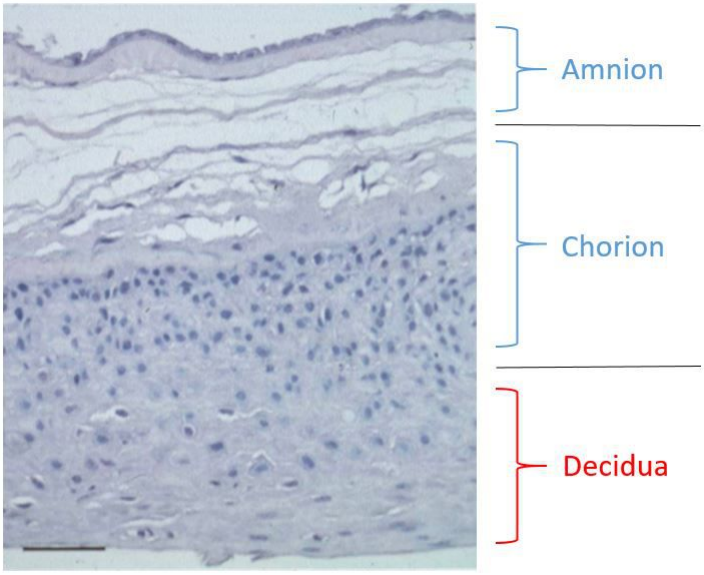

Figure 2.2: The fetal membranes and decidua layers during pregnancy [15].

While the CA membrane is composed of many layers, the connective tissue it contains is of primary importance [14]. This connective tissue, similar to connective tissues amongst other parts of the body, provides the structural mechanical properties of fetal membranes, such as strength and elasticity [14]. Although the amnion is typically 150 μm thinner than the chorion, its makeup of collagen fibrils provides it with much more strength than the chorion [14]. As fetal membrane rupture is essential for childbirth, it is important that rupture of the CA occurs, naturally or artificially, at full-term. Although failure of fetal membranes occurs for many reasons, the most common mode of failure tends to be associated with mechanical events [14]. Researchers have attempted to perform three different types of mechanical tests on fetal membranes, including uniaxial tensile tests, biaxial burst tests, and planar biaxial testing [14]. Although each of these tests provide both qualitative and quantitative data, the testing that has been used for this project is biaxial puncture testing because it is the most accurate representation of how the fetal membranes are loaded and punctured in the body. This method of testing provides the failure strength of the membranes, which in turn, provides the elastic modulus with consideration of the membrane thickness. Prior

to now, there has never been biaxial puncture testing on fetal membranes. These mechanical properties are essential to develop a membrane patch used to treat PPROM. Researchers in previous studies have concluded that the failure strength of CA membranes is approximately 0.9 MPa [14].

2.1.2 Cervix and Cervical Insufficiency

The cervix makes up the lower portion of a woman's uterus. The cervix is lined internally by the endometrium and the decidua, which are overall weak tissues [16]. The relationship between the biochemical factors and the biomechanical properties within the body is a difficult, yet crucial, assessment to understand [17]. Over the course of pregnancy, cervical tissue begins to soften while the cervix ripens, or thins, to prepare for birth [17]. Cervical ripening refers to the structural changes occurring within the cervix, such as tissue changes and external loads (contractions, pressure, uterine growth, adhesion between membranes) [17]. Many of the mechanical failures that occur within the cervix are due to its extracellular matrix (ECM) [17]. Cervical ECM is composed of many elements, with two of the most significant being hyaluronic acid (HA) and fibrillar collagen [17]. The amount of HA helps regulate the hydration in the cervical tissue which results in enhanced mechanical properties [17]. This, in turn, plays a significant role in cervical ripening [17]. Cervical collagen is composed of fibrillar collagens type I and type III, which provides the cervix with strength [17]. The hierarchical structure of collagen fibers plays a crucial role in the mechanical properties of the cervix [17]. In some cases, a polymorphism of collagen type I occurs and plays a significant role in cervical insufficiency and cervical softening [17]. Many studies have been conducted to compare cervical tissues of pregnant and non-pregnant women. The results of these studies show that the cervix of a pregnant woman is much softer and less stiff than that of a non-pregnant woman [17]. Researchers have concluded that chorioamnionitis and decidual hemorrhage can play a significant role in the weakening of a cervix, as well [17]. It is believed that the crosslinking of collagen fibers can strengthen the cervix and enhance its mechanical properties [17].

Cervical insufficiency occurs when the woman's cervix begins to dilate preterm prior to the onset of labor [6]. If preterm cervical dilation occurs, then this could lead to immediate pregnancy loss [6]. In cases of cervical insufficiency, CA membranes are stretched and possibly cause the cervix to form an hour-glass shape, thus pregnancy loss inevitably occurs if medical treatment is not obtained immediately [6]. Although medical treatment can help prevent pregnancy loss in these cases, the damage to the membranes gone cannot be fully healed and can ultimately result in mechanical failure of the CA [6]. As fetal membranes are in contact with the cervix, the membranes also become exposed to the outside world if the cervix begins to open preterm, which increases the chance of PPROM. If cervical insufficiency occurs and membranes begin to mechanically fail, then a cervical cerclage is often the method used to prevent preterm birth. During a cervical cerclage, a suture is located appropriately to close the cervix, in order to prevent PPROM and PROM (Figure 2.3)[6].

2.2 The Importance of Collagen

Collagen protein is a vital part of the body as it affects the health of one's joints and the elasticity of skin [18]. Collagen is located throughout the entire body making it the most abundant protein in the human body [18]. Collagen fibers are composed of several layers of structure, including fibrils, microfibrils, and polypeptide chains with amino acids, as can be seen in Figure 2.4 [20].

As collagen is an important part of the connective tissue of the body, it is especially vital during pregnancy. Collagen fibers play a significant role in the elasticity of fetal membranes, similar to how collagen provides elasticity to the skin. The chorioamnion layer surrounding the fetus is composed of many sub-layers, with one of the most critical being a collagenous matrix in the compact layers as seen in Figure 2.5 [21]. These strong collagen fibers help protect the fetus from harmful substances, such as infectious diseases, and keep the amniotic fluid within the sac

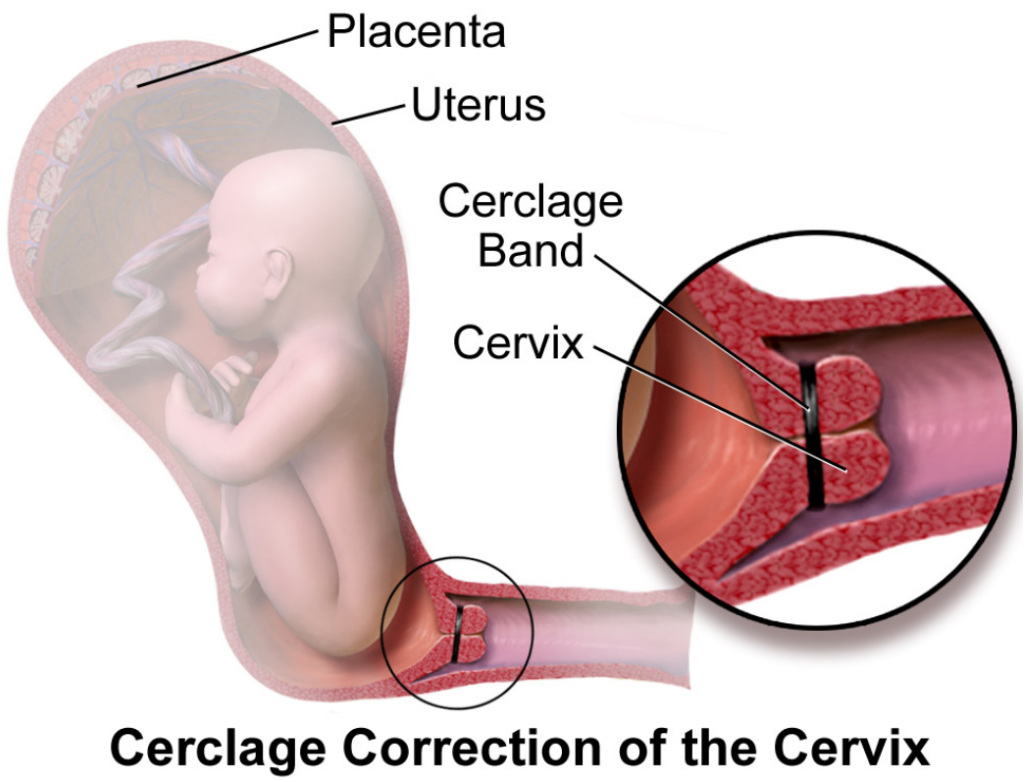

Figure 2.3: A cervical cerclage to prevent preterm birth after PPROM occurs during cervical insufficiency [19].

[21]. Although the chorion is composed of different types of collagen, the amnion layer has a greater amount of these collagen types; for example, the chorion contains collagen type I and type III, which plays a large role in the mechanical integrity of the amnion layer, providing stiffness and strength [21]. Due to amnion strength impacting the occurrence of PPROM, it is the primary layer of focus throughout this project. Figure 2.5 provides a descriptive schematic of the many extracellular-matrix components within the chorion and amnion layers.

Because collagen fibrils have such a large impact on the mechanical properties of fetal membranes, it is important that they remain strong and supportive throughout the duration of pregnancy. Sadly, this is not always the case. When a pregnant woman acquires an infection or has inflammation, protein enzymes, such as collagenase, begin to form from both the woman's immune system

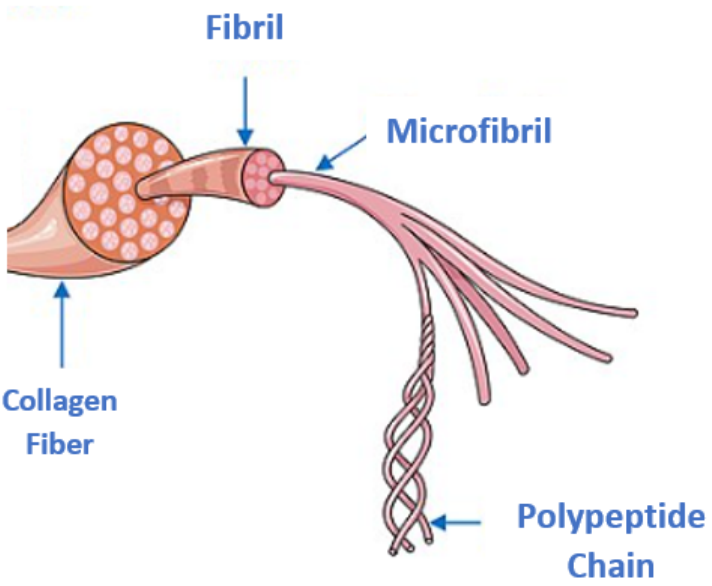

Figure 2.4: Anatomical structure of a collagen fiber into fibrils and collagen molecules [20].

and the infection site. These collagenase enzymes attack the collagen fibrils of the CA causing them to degrade and convert from a triple-helix to single peptides, essentially leading to the weakening of fetal CA membranes [22]. This process is thought to be a leading cause in the preterm pre-labor rupture of membranes. Figure 2.6 displays a schematic of the degradation collagenase causes on collagen fibers.

2.3 Biomimetic Materials

After discussing natural anatomy of pregnancy, it is also important to understand how research regarding this topic is evolving and focusing on biomimetic materials. Biomimetic materials are products that are fabricated through merging artificial substances with biologically produced materials and biological processes [2]. Biomimetics is a growing field as it has the ability to fabricate materials to embody self-healing and hydrophobicity characteristics. Two prime examples of biomimetic materials are hydrogels and electrospun fiber mats. Both of these biomimetic materials are capable of cell injection to enhance self-healing in the body. The field of biomimetics was

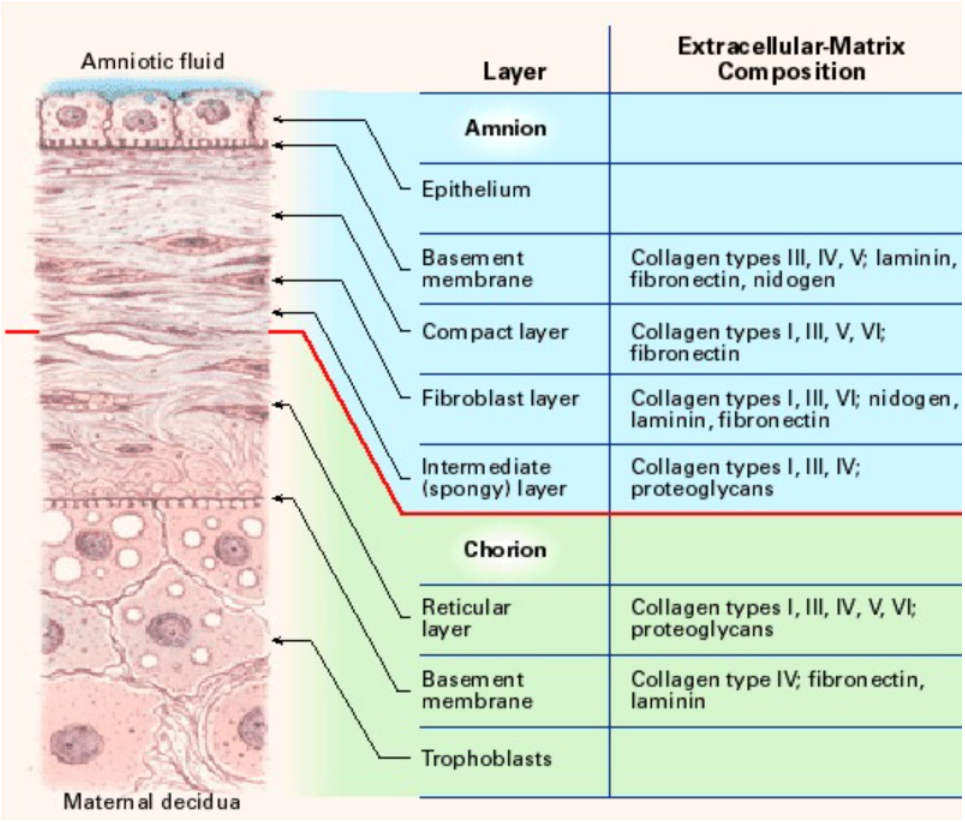

Figure 2.5: The collagen types that comprise the chorion and amnion layers [21].

implemented throughout this project with tissue repair being the ultimate goal of using an artificial biomimetic membrane.

2.3.1 Hydrogels

Hydrogels have recently gained more attention within the last two decades due to their ability to react with cells and bioactive molecules to regenerate lost or damaged tissues [23]. As the human body is composed of 80% water, hydrogels also contain a massive portion of water, making them extremely biocompatible. Hydrogels are often used in tissue engineering to create scaffolds due to their hydrophilic properties and their ability to mimic biological substances [24]. Figure 2.7 displays the a schematic of the crosslinking properties of hydrogels.

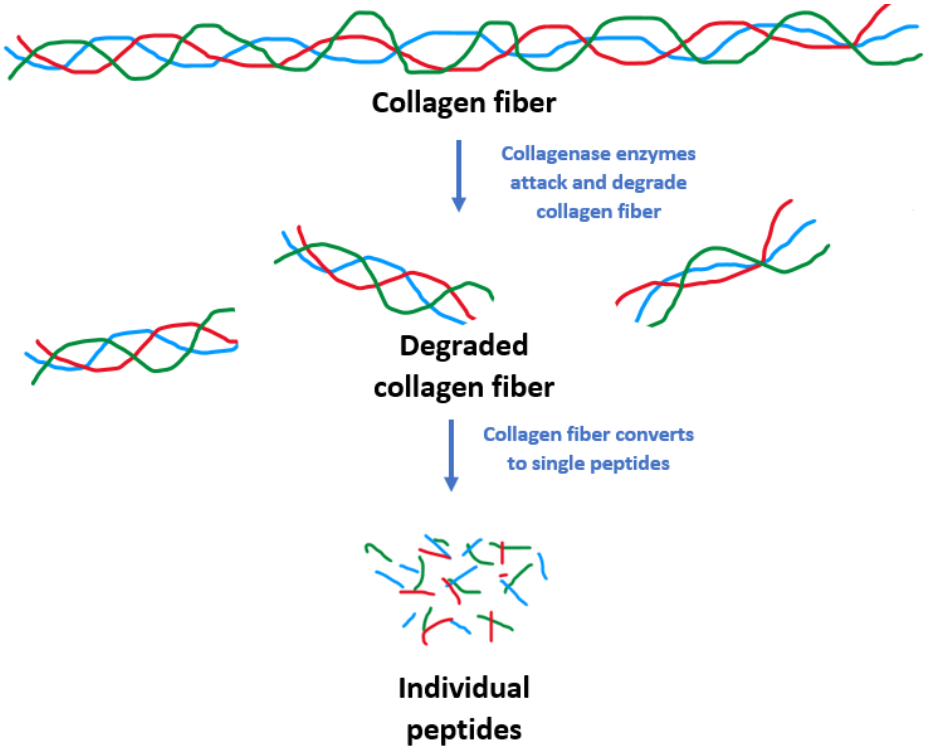

Figure 2.6: The degradation that occurs when collagen is exposed to collagenase [22].

Hydrogel beads provide a great amount of mechanical strength compared to biological tissues and can integrate within the native ECM of the human body by fusing with living cells and bioactive factors [23],[24]. Due to a lack of organ donors and highly biocompatible property of hydrogels, hydrogels have become used for transplantation into humans in order to mimic damaged tissues [23]. The goal of hydrogel insertion is to inject viable cells into the scaffold, leaving only the cells to regenerate healthy tissues once the hydrogel scaffold eventually degrades [23]. Although hydrogels are often used as compatible biomimetic materials, the elastic modulus of hydrogels are in the kilopascal (kPa) range, whereas the elastic modulus of collagen fibers are typically in the megapascal (MPa) range. Therefore, electrospinning fiber mats known to have a greater stiffness were selected as the biomimetic materials for this study.

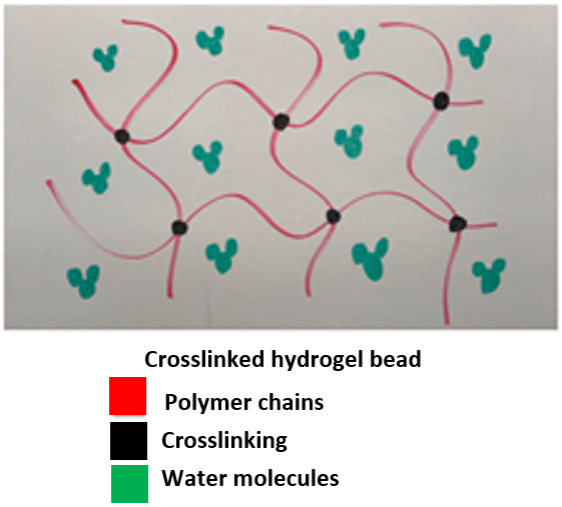

Figure 2.7: Schematic of crosslinking that occurs in hydrogels.

2.3.2 Electrospinning Nanofibers

In the early 1930s, Anton Formhal developed the concept of electrospinning, which became highly popular in biomedical engineering in the early 2000s as it is greatly relevant in the creation of implantable scaffolds and cell rejuvenation [25], [26], [27], [28] and [29]. By applying electrostatic forces, electrospinning produces fibers that measure on the nanometer scale [27], [30]. High voltage sources are utilized to project polymer solutions onto a platform that serves as a ground electrode collector [27]. Electrospun fiber mats consist of a small pore size and have diameter sizes that range from 100 nm to 500 nm [27], [30]. Figure 2.8 exhibits a representation of the electrospinning process which includes a syringe pump that propels the polymer solution towards a collector screen using a high voltage source controlling the nanofibers [27]. Evaporation of the liquid solution occurs as the polymer solution travels towards the collector screen and transforms the polymer solution into a solid fiber mat [31]. This project relied on electrospinning because the gelatin fibers produced were highly similar to human collagen fibers. The comparison of collagen fibers to electrospun gelatin fibers can be seen in Figure 2.9, where gelatin is simply a denatured version of collagen and highly biocompatible.

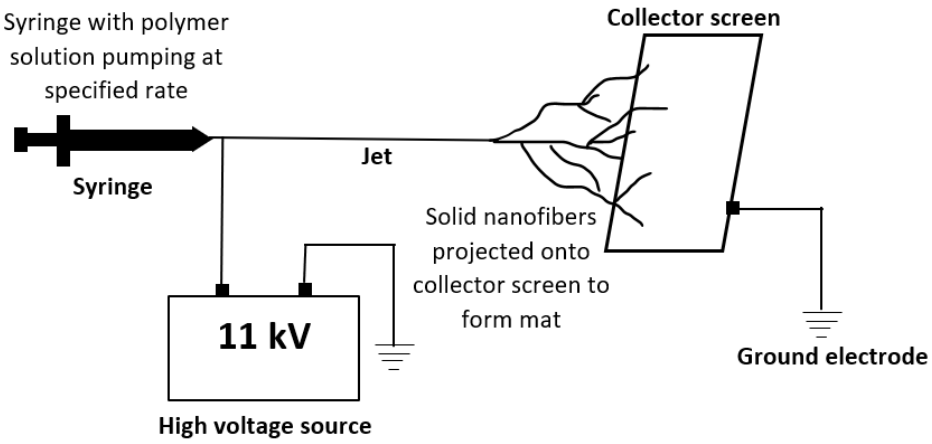

Figure 2.8: Detailed schematic of the electrospinning process [27].

This chapter included a summary of natural fibers in the placenta and also focused on the artificial biomimetic materials that have previously and currently been used as biomedical engineering applications. The testing data from this project, including nanoindentation of hydrogels will now be examined.

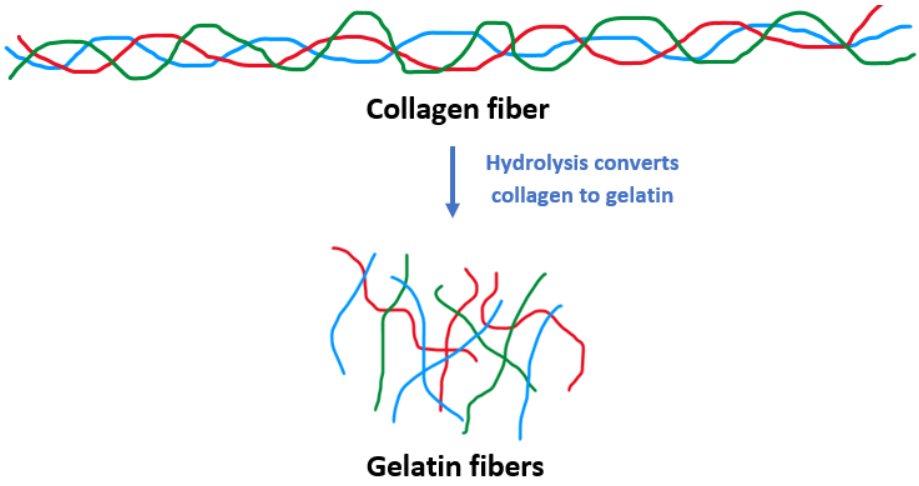

Figure 2.9: Comparison of collagen fibers and gelatin fibers [32].

CHAPTER 3

NANOINDENTATION TESTING

3.1 Introduction

Nanoindentation is a method used to analyze the mechanical properties of hydrated materials, including biological tissue [33], [34]. This method evolved in the 1980's and has been widely used ever since [34]. Nanoindentation is a method of mechanical testing on the nanoscale as it also involves the process of physically contacting the specimen being tested. Once the nanoindenter probe is in contact with the specimen, it continues lowering, typically tens to hundreds of nanometers, until the specified indentation depth is met. The force that is being applied to the specimen, the displacement the probe makes to reach the specimen, and the time the probe is in contact with the specimen can all be obtained throughout the duration of testing. The primary difference between nanoindentation testing and mechanical testing on the macro scale is the act of not fully rupturing a sample during nanoindentation, but instead, only indenting. A schematic of nanoindentation testing is shown in Figure 3.1. This portion of the project is to validate the stiffness of two biomimetic membranes (Matrigen® hydrogels and polyacrylamide hydrogels).

3.2 Methods

An Optics 11 nanoindenting machine was used to conduct nanoindentation tests. Matrigen® hydrogel samples, with expected elastic modulus values of 4 kPa, 12 kPa, 25 kPa, and 50 kPa were tested after being swelled in saline contact lens solution for approximately 48 hours. These stiffness values were selected due to the availability of gels in the laboratory. Because the stiffness

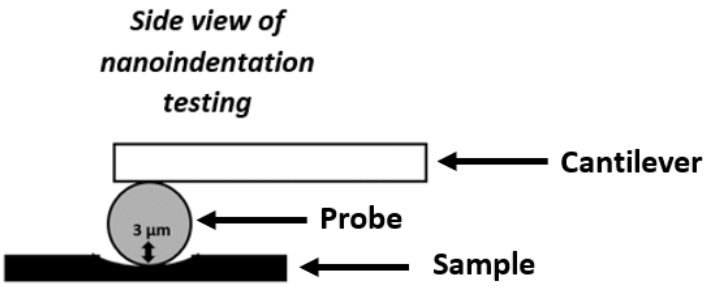

Figure 3.1: Side view of a nanoindentation test.

of the gels were already known, this testing was conducted to create calibration standards and to validate the process of testing on a small scale compared to values from traditional techniques on larger scales. Calibration of the probe in the air and liquid contact lens solution was conducted before using the machine each time. After calibration, the probe stayed submerged in the contact lens solution for approximately 15 minutes. Once the testing specimen was placed under the probe on the home stage, the probe stayed completely submerged in the liquid throughout the entirety of testing. Indentation depths of 2 µm, 3 µm, 4 µm, and 5 µm were tested for the Matrigen® hydrogels. For each indentation depth, a 4x4 matrix scan was set up to allow 16 total tests to be conducted per depth. Figure 3.2 shows the machine used for nanoindentation and an enlarged view of the micrometer-sized probe used to indent the samples. A variety of probe sizes were used to test the Matrigen® gels due to probes breaking frequently, which is suspected to be due to Optics 11 manufacturing.

After testing Matrigen® hydrogels, polyacrylamide hydrogels were fabricated and tested in the same manner with the Optics 11 nanoindentation machine. Gels with 1 kPa, 10 kPa, and 50 kPa elastic modulus values were fabricated in lab. These values were chosen to ensure a large range of stiffness values were fabricated and tested. Table 3.1 lists the weight percentages of the materials used for each polyacrylamide gel stiffness.

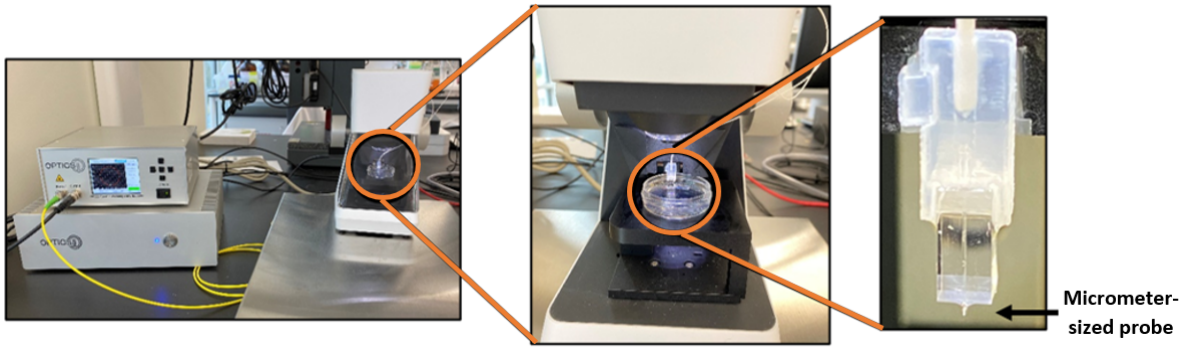

Figure 3.2: Typical Optics 11 nanoindentation testing setup and probe that is submerged into the testing solution.

Table 3.1: Material weight percentage for each polyacrylamide gel stiffness.

Stiffness of Hydrogel (kPa)	**Potassium Persulfate (PPS) (%)**	**TEMED (%)**	**Phosphate Buffered Saline (PBS) (%)**	**Acrylamide (%)**	**Bis (%)**	**Distilled Water (%)**
1	7.5	7.5	10	7.5	0.013	55.6
10	7.5	7.5	10	7.5	0.07	52.8
50	7.5	7.5	10	8	0.75	14.3

All chemicals came from Millipore Sigma (MilliporeSigma, Burlington, MA), aside from the acrylamide and bis from BIO-RAD (BIO-RAD Laboratories, Hercules, CA). Once the polyacrylamide solutions were prepared, the gels were placed in petri dishes on glutaraldehyde-treated glass coverslips that were shipped from the University of Columbia. The glutaraldehyde coverslips acted as a chemical crosslinker that allowed the acrylamide to bind to the glass. This binding ensured that the gels stayed in place in the petri dish. Once polymerized, saline solution was poured into the petri dish to allow the gel to be submerged and to swell. Due to the toxic monomers of the acrylamide used in the gels, the saline solution was discarded and changed every 8 hours for a total of 48 hours.

After fabrication and swelling of the polyacrylamide gels were complete, testing began. The probe used for this polyacrylamide testing had a radius of 99 μm and a stiffness of 0.51 N/m. A total of three 50 kPa gels, two 1 kPas and two 10 kPa gels were tested. Due to this testing being done on a nanoscale, a wooden box surrounded the machine throughout the entirety of each test to alleviate any external noise or movements that could cause the probe to move and result in inaccurate data. Three indentation depths were tested per polyacrylamide gel: 3 μm, 4 μm, and 5 μm. These indentation depths were chosen based on preliminary studies. For each indentation depth, a 4x4 matrix scan was set up to allow 16 total tests to be conducted per depth.

For both the Matrigen® and polyacrylamide gels, the probe was lowered 10 μm to the surface of the hydrogel, indented the hydrogel for 15 seconds, and moved back up to the starting position 10 μm above the sample. Once the probe was completely out of contact with the hydrogel surface but still submerged in the liquid, the home stage was set to move 100 μm in both the x- and y-direction before indenting again.

After testing of all gels (both Matrigen® and polyacrylamides) was complete, they were all analyzed in the same manner to allow the elastic modulus to be obtained.

3.3 Results

Although not each of the samples tested are displayed, examples of representative curves for three different stiffness values at a 3 μm indentation depth can be seen in Figure 3.3. Regarding the load as a function of time graphs, it can be seen that there is a rapid increase in load until approximately three seconds when it begins to stabilize throughout the duration of indenting. The maximum load differences for each gel stiffness should also be noted. For each gel stiffness, the probe becomes unloaded between 15 and 20 seconds when the probe returns to its starting position at load zero.

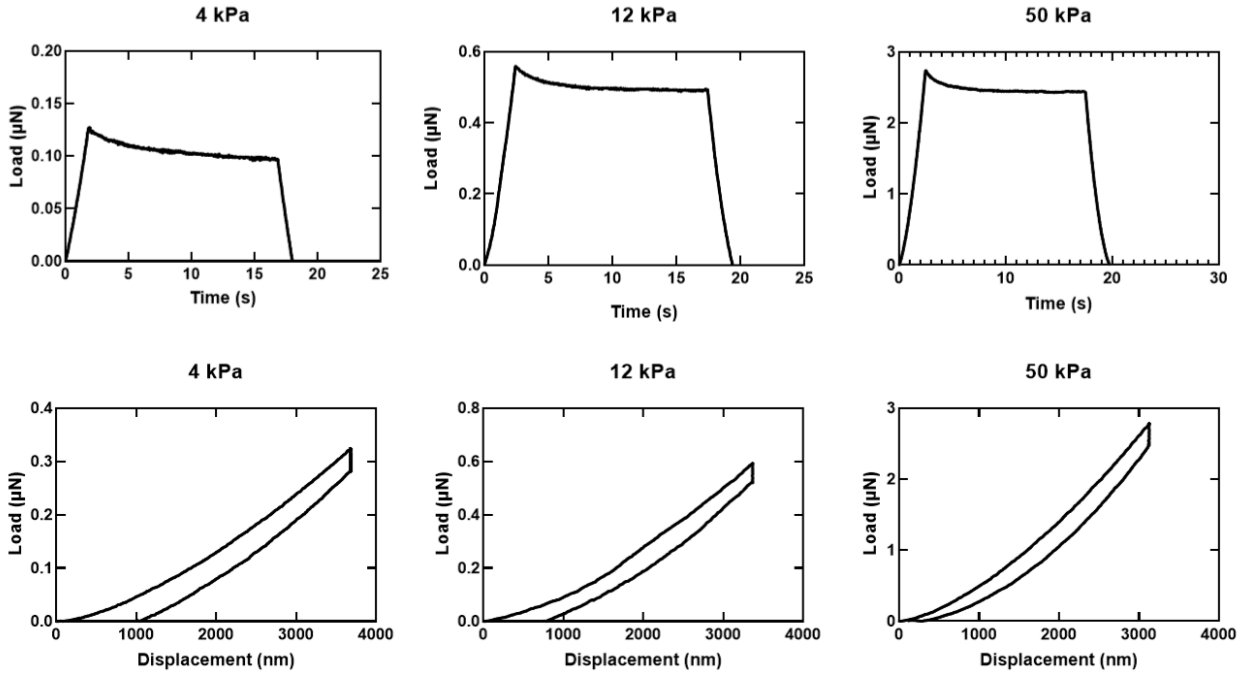

Figure 3.3: Representative plots for 4, 12, and 50 kPa Matrigen® hydrogels after nanoindentation testing.

The results for the Matrigen® hydrogel study are shown in Figure 3.4, while the results for the polyacrylamide study are shown in Figure 3.5.

3.4 Discussion

This portion of the study was to validate the stiffness of two biomimetic membranes (Matrigen® hydrogels and polyacrylamide hydrogels). As shown in Figure 3.4, each Matrigen® hydrogel stiffness was significantly lower than the anticipated value. The gel that had measured values closest to its anticipated value was the 4 kPa Matrigen® gels. Although several different sized probes had to be used for the Matrigen® gels, it is clear within the data that the values remained relatively consistent regardless of probe size.

There is minimal data within the literature that studies the mechanical properties of materials with elastic moduli values in the kPa range through nanoindentation testing; additionally, there are

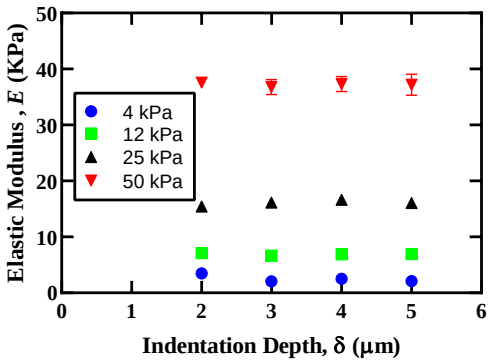

Figure 3.4: Elastic modulus as a function of indentation depth for Matrigen® hydrogel study.

no previous studies with calibration standards for this method. Therefore, this collaboration was conducted to assess validity and reproducibility of the techniques for future testing on biological tissues in low stiffness regimes.

The results of the polyacrylamide hydrogel testing showed that the elastic modulus of each gel was relatively similar to that of its anticipated stiffness, except for 50 kPa gels. While the 1 kPa

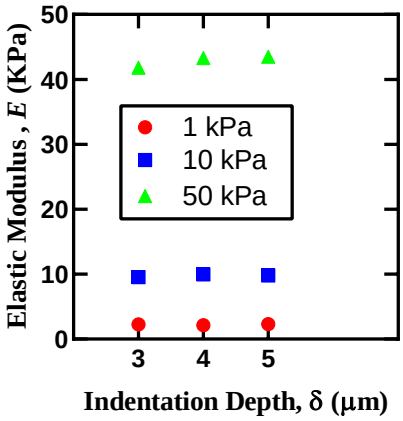

Figure 3.5: The elastic modulus as a function of indentation depth for the polyacrylamide gels .

and 10 kPa gels were consistent as the indentation depth changed, the 50 kPa gels showed minimal variation, but slightly increased in stiffness as indentation depth also increased.

This chapter focused on the small experiment that was conducted to create a calibration standard for mechanical testing on a nanoscale. This was completed by mechanically testing hydrogels with known elastic modulus values, indicating that the majority of the Matrigen® gels measured lower than the anticipated value while only the 50 kPa polyacrylamide gels measured lower than anticipated. The 1 kPa and 10 kPa polyacrylamide gel values were consistently their respective anticipated values. This next chapter will discuss the methods implemented to electrospin nanofibers and the process of how these fiber mats were mechanically tested.

CHAPTER 4

ELECTROSPINNING STUDY

4.1 Introduction

Hydrogels are often used as biological tissue replacement. But, without a strong and compact matrix, they cannot withstand the external loads placed on them within the human body [35]. Therefore, electrospinning is a cost-efficient method that has been applied for decades and can be used to reinforce the hydrogel with its nanofiber matrix to allow it to withstand external forces [35]. Electrospun fiber mats are known to have high porosity and have similar properties to the extracellular matrix of cells [36]. There are many parameters involved in electrospinning, including diameter size, nanofiber location, and fiber morphology. Having many effective parameters can serve as both beneficial and harmful [29]. For example, having numerous parameters allows researchers to adjust different factors in order to receive specific results, such as voltage source, working distance, and pump rate. Furthermore, many parameters can also make it difficult for the process to be repeatable, which is important in biomedical engineering [29]. Thus, the second part of this project focused on the creation of electrospun biomimetic membranes (two gelatin polymer solutions: uncrosslinked and crosslinked electrospun fiber mats) that can be used as a model system for research purposes and thus a potential repair patch for a placental rupture site in instances of preterm rupture of membranes.

4.2 Methods

Two gelatin polymer solutions were prepared for the electrospinning process: uncrosslinked and crosslinked. The materials used for this study were gelatin from porcine skin with a 300

g bloom strength, acetic acid, sodium hypophosphite (SHP), and citric acid [37]. Gelatin at 12 weight percent was dissolved in a 9:1 ratio by weight acetic acid and distilled water to create uncrosslinked fiber mats [37]. The crosslinked solution was made in the same manner, but with the addition of 7.5% SHP and 15% citric acid [37]. All chemicals were obtained from Millipore Sigma (MilliporeSigma, Burlington, MA), aside from the acetic acid which was from VWR (VWR International, Radnor, PA). These polymer solutions were electrospun using the Spraybase® Electrospinning/Spraying Starter Kit, as shown in Figure 4.1. The ejector needle was placed 12.5 cm from the collector screen while a voltage of 11 kV was applied to the solution. The polymer solution was spun for 7 hours at a rate of 0.3 mL/hr [37]. A visual representation of the polymer solution leaving the needle and undergoing a high voltage can be seen in Figure 4.1. As the solution left the needle and a high voltage was applied, the liquid solution converted to a solid fiber which was spun onto a collector screen. A total of 16 mats were electrospun. Four uncrosslinked and four crosslinked mats were placed in the oven at 150 °C for four hours. After the four hours, the heat-treated mats and the remaining eight mats were placed in the desiccator until testing began. Therefore, the four categories of electrospun fiber mats that were tested include 4 not treated crosslinked (NX), 4 not treated uncrosslinked (NU), 4 treated crosslinked (TX), 4 and treated uncrosslinked (TU) where "treated" indicates that they were heated in the oven.

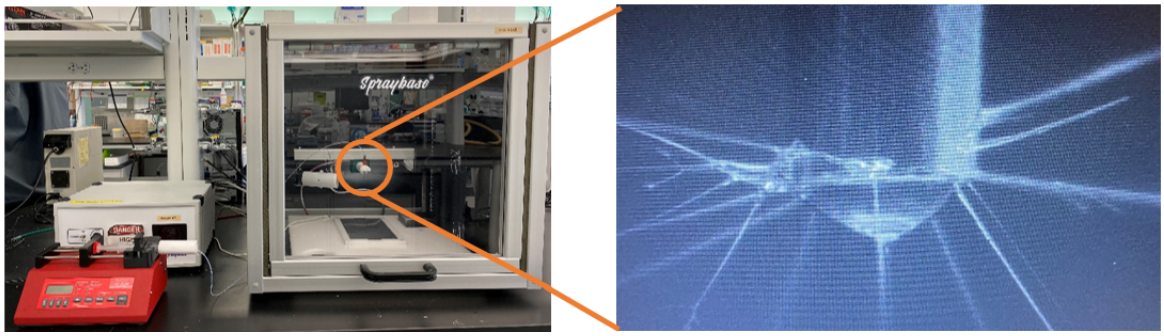

Figure 4.1: The Electrospinning machine used for this research project and the polymer solution leaving the needle tip as a liquid is converted into a solid fiber.

Aluminum was used as the collector screen to catch the fibers as it is a conductive material. The fibers spun perfectly on the sheet of aluminum, as shown in part A of Figure 4.2. Although the aluminum is a great conductive material to spin onto, it was noted that the fiber mat could not be easily removed from the aluminum as the fiber mat stuck to the sheet after spinning. Next, several different 3D printed shape cutouts and a glass slide were placed on the aluminum. Figure 4.2 parts B, C, and D show that the fibers did not spin well onto these materials due to either the fibers sticking to the material (glass slide in part B) or the height of the cutouts (6 mm) were too thick, and the fibers caved into the cutout (parts C and D). The next idea was to place a rectangular Teflon cutout on top of the aluminum. As can be seen in part E of Figure 4.2, the fibers spun nicely onto the Teflon material, but only for a brief time until the fibers began spinning on other pieces of metal within the machine. It is suspected that because there were no hole cutouts in the Teflon material and due to its thickness (1.5 mm), there was not enough exposed aluminum for the material to spin appropriately.

Finally, large sheets of non-stick Teflon at a much smaller thickness (0.06 mm) with hole cutouts were obtained and placed on top of the aluminum. The hole cutouts allowed there to be enough aluminum for the fibers to attach to the collector screen. The fiber mat shown in Figure 4.3 was electrospun for approximately 4 hours and easily peeled off of the non-stick Teflon material. Figure 4.3 shows the fiber mat spun onto the thin Teflon with hole cutouts and the mat completely removed from the collector screen. This material and method was the best fit for this project and is what was used to spin all 16 fiber mats that were tested.

Final electrospun fiber mats ranged between 140-180 mm in length and approximately 80-115 mm in width. Once a nanofiber mat was electrospun, it was cut into approximately 30 mm $\times$ 30 mm squares and placed between 3D printed grips with a 20 mm diameter cutout. Sandpaper was glued to the interior of the grips to prevent the specimen from slipping. Once the samples were placed between the grips, they were held together by binder clips. The final product of the samples between the grips and placed on the machine for testing is shown in Figure 4.4.

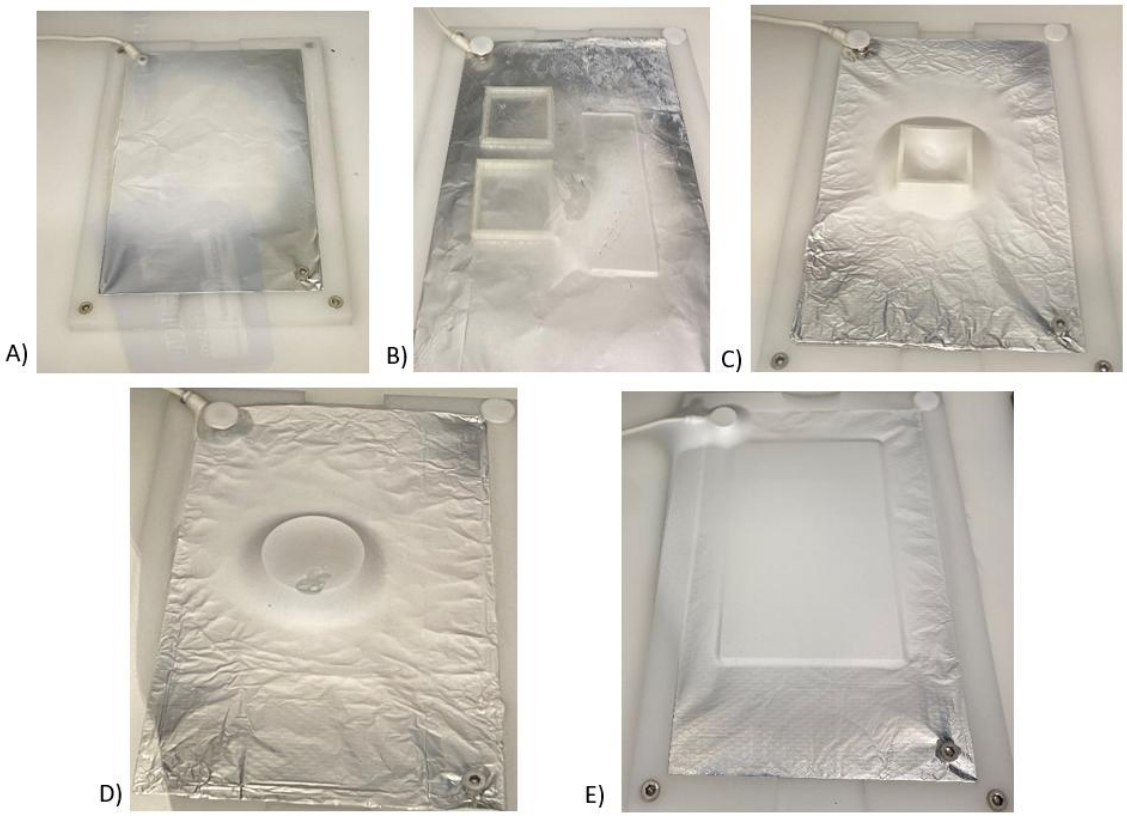

Figure 4.2: Several attempts to find the perfect material for the polymer solution to electrospin appropriately. A) Spinning directly on aluminum B) and C) Spinning on 6 mm thick 3D printed square cutouts and on a 1 mm thick glass slide D) 6 mm thick 3D printed circle E) 1.5 mm thick rectangle Teflon cutout without holes.

4.2.1 Electrospinning Mechanical Testing

An overhead view of a fully punctured sample placed between the grips with a 20 mm cutout is shown in Figure 4.5. Using a 200 N load cell, a puncture test was set up using the Zwick Roell machine, as seen in Figure 4.4. For each test, a 3.5 mm diameter probe was set to lower at a rate of 0.5 mm/s until a load of 0.01 N was applied to the sample and dwell for 120 seconds. After dwelling, the probe continued lowering until failure occurred and returned back to its original position. A schematic of the testing process is displayed in Figure 4.5. The Zwick Roell machine

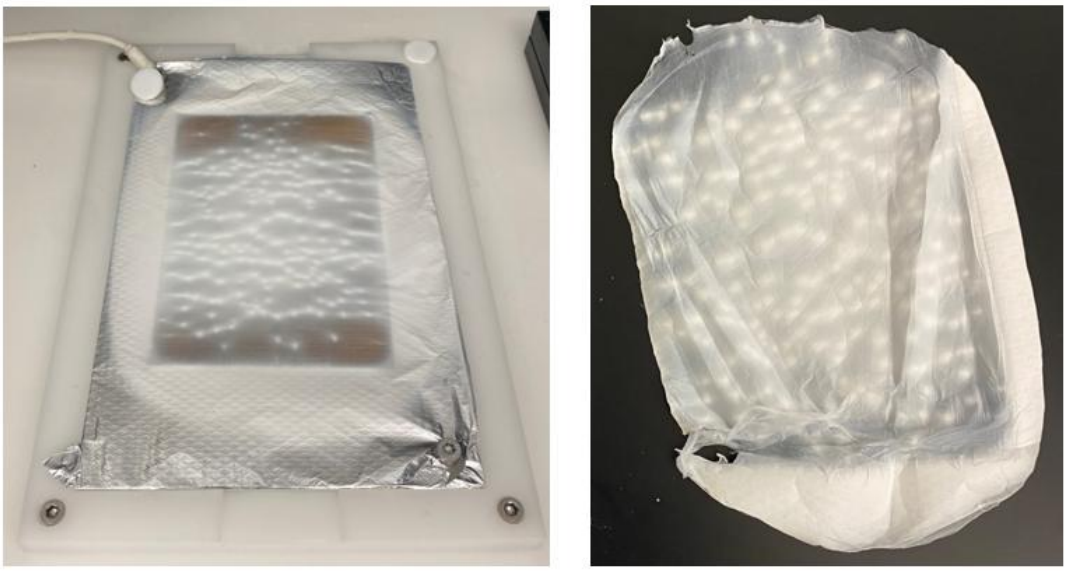

Figure 4.3: Final electrospinning material setup with easily removable fiber mat.

provided the load and displacement that occurred during testing. An example of a fully tested fiber mat can be seen in Figure 4.5 (right side).

Due to the load and displacement being obtained through testing and the thickness of the specimen being measured prior to testing, the elastic modulus, E, could be calculated using Equation 4.1.

$$E = \frac{16a^{\frac{9}{4}}F_{MAX}}{9\pi h x^3 R^{\frac{1}{4}}} \tag{4.1}$$

in which a is the specimen holder radius, F_{MAX} represents the puncture force when the sample fails, h is the thickness of the membrane, x is the displacement in the z-direction, and R represents

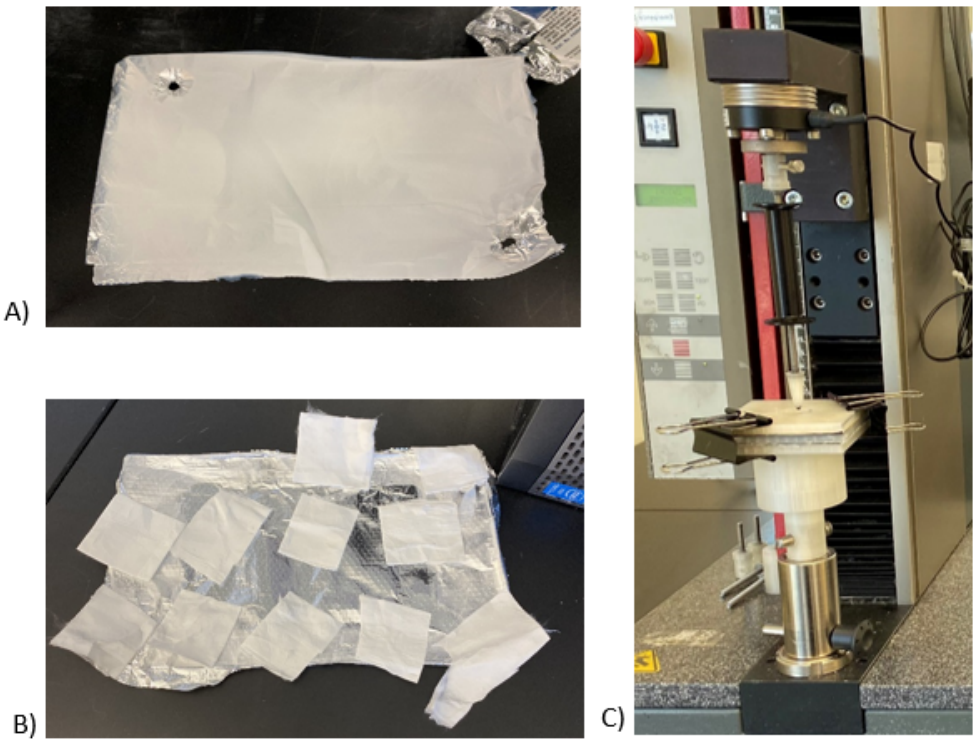

Figure 4.4: A) Electrospun fiber mat after 7 hours of spinning B) Electrospun fiber mat cut into 30 mm $\times$ 30 mm pieces to prep for testing C) A 30 mm $\times$ 30 mm fiber mat cutouts placed between the grips and placed on the Zwick Roell machine for testing.

the probe radius [12]. After the elastic modulus was calculated for each sample, this value was then used in Equation 4.2 to obtain the failure strength, σ, of the specimen.

$$\sigma = \frac{1}{h}\sqrt{\frac{F_{MAX}Eh}{6\pi R}} \tag{4.2}$$

in which these variable values correspond to the variables used in Equation 4.1 [38]. The average and standard deviation elastic modulus and failure strength for each test was calculated.

4.2.2 Electrospinning SEM Imaging

Two of the largest contributors to a sufficient scanning electron microscope (SEM) image is the voltage and current that are applied. Different scenarios of voltage/current ratios, such as high

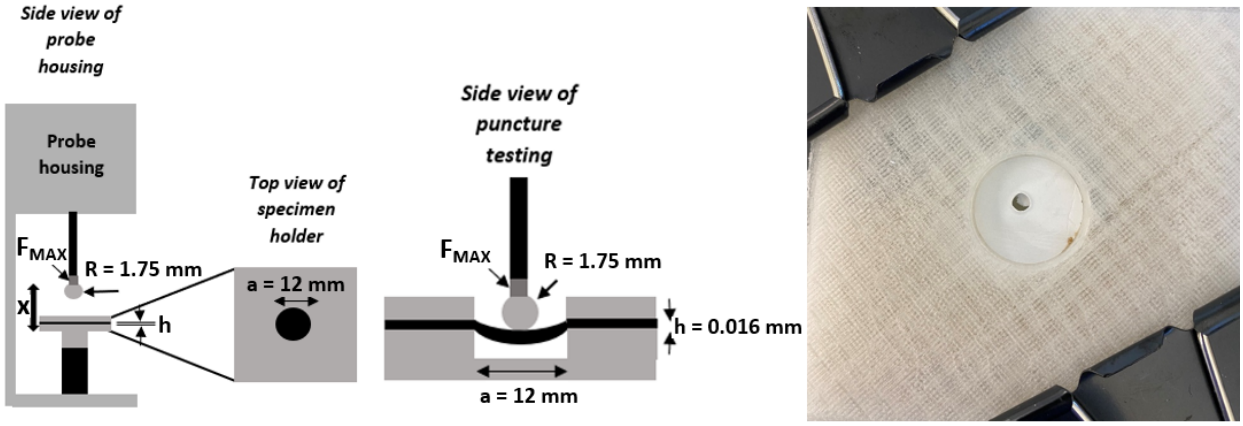

Figure 4.5: A schematic of the testing process, along with a fully punctured electrospun fiber mat.

voltage/high current, high voltage/low current, low voltage/high current, and low voltage/low current were imaged to obtain the proper combination that created the clearest image. These different ratio images can be seeing in Figure 4.6 and were each obtained at a constant magnification of 5.00k.

4.3 Results

4.3.1 Electrospinning Mechanical Testing

The raw data of all four fiber mat categories is displayed in Figure 4.7, with the majority of samples failing between a displacement of 4-6 mm for the uncrosslinked fiber mat (both treated and untreated) and 1-3.5 mm for crosslinked (both treated and untreated). Loads up to approximately 20 N were reached for the uncrosslinked fiber mats, while only approximately 1-5 N was obtained for the crosslinked fiber mats.

Once raw data was obtained and data analysis was conducted, there were significant differences in the elastic modulus and strength values for each category, which can be seen in Figure 4.8. An average elastic modulus of less than 250 MPa was obtained across the board for each category, while there were significant differences in the strength values. Strength values for the

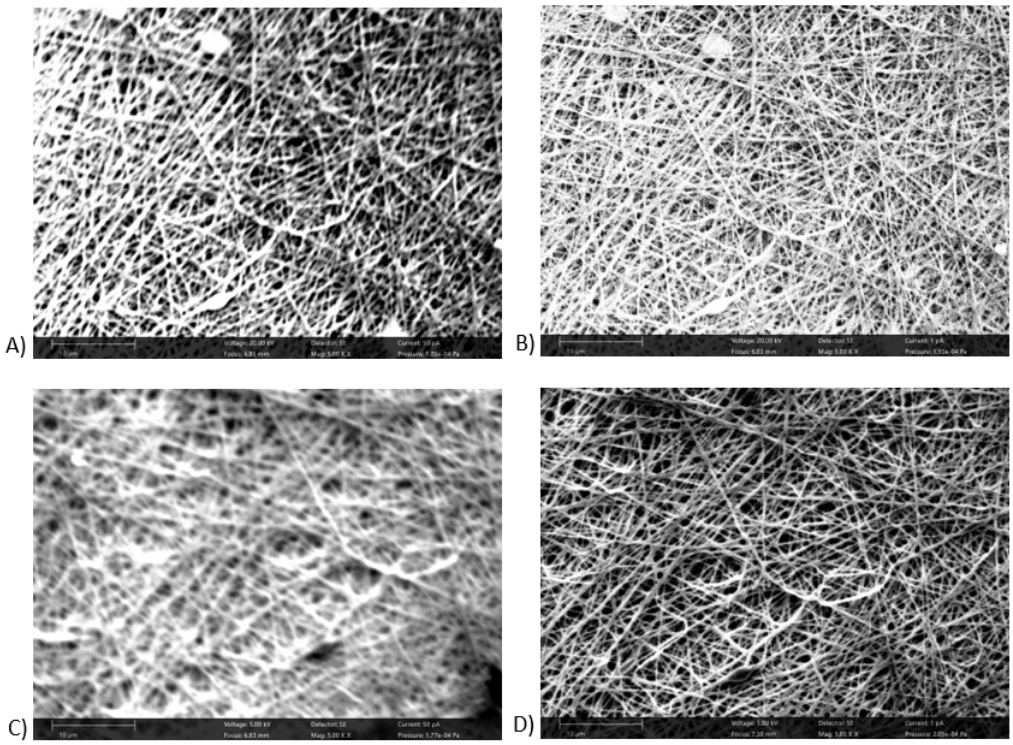

Figure 4.6: A) High voltage/high current B) High voltage/low current C) Low voltage/high current D) Low voltage/low current.

uncrosslinked fiber mats were approximately 10 MPa while the crosslinked fiber mats were lower than approximately 5 MPa.

The elastic modulus and strength values demonstrated a clear trend. Therefore, Figure 4.9 illustrates the differences in mechanical properties between the four different electrospun fiber mat types.

The final SEM image for each electrospun fiber mat category was obtained with the low voltage/low current combination at a magnification of 5.00k, which resulted in a scale of 10 μm. The reason for obtaining SEM images of the mats was to understand the fiber morphology at a high magnification. The final SEM images can be seen in Figure 4.10.

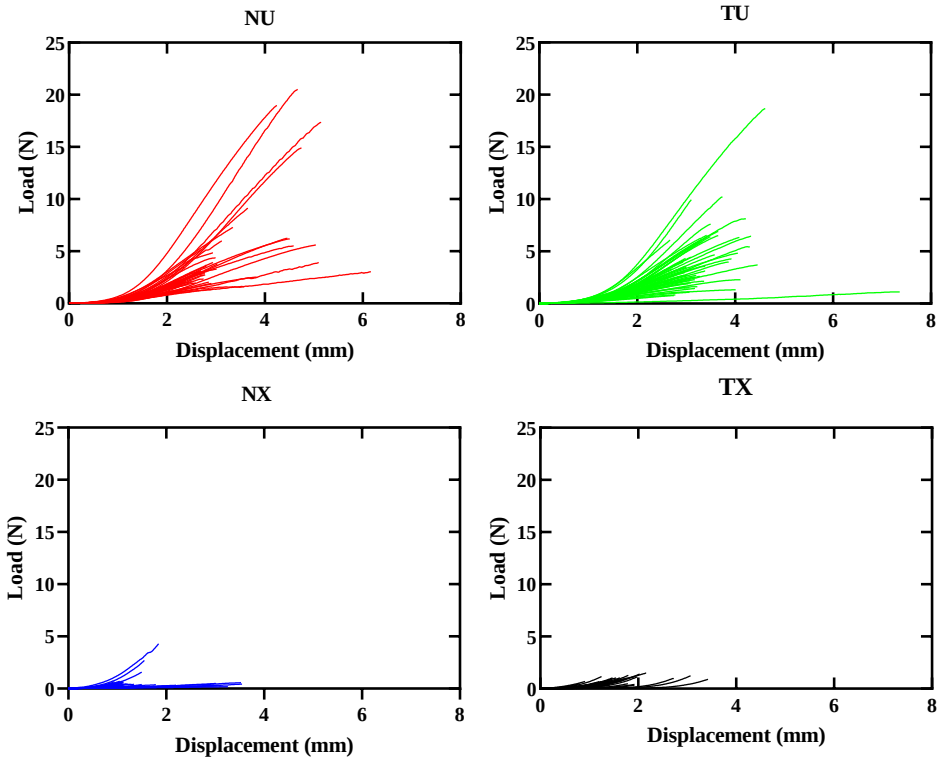

Figure 4.7: Raw data of maximum load as a function of displacement for each of the 4 fiber mat categories tested. Each line represents each sample tested.

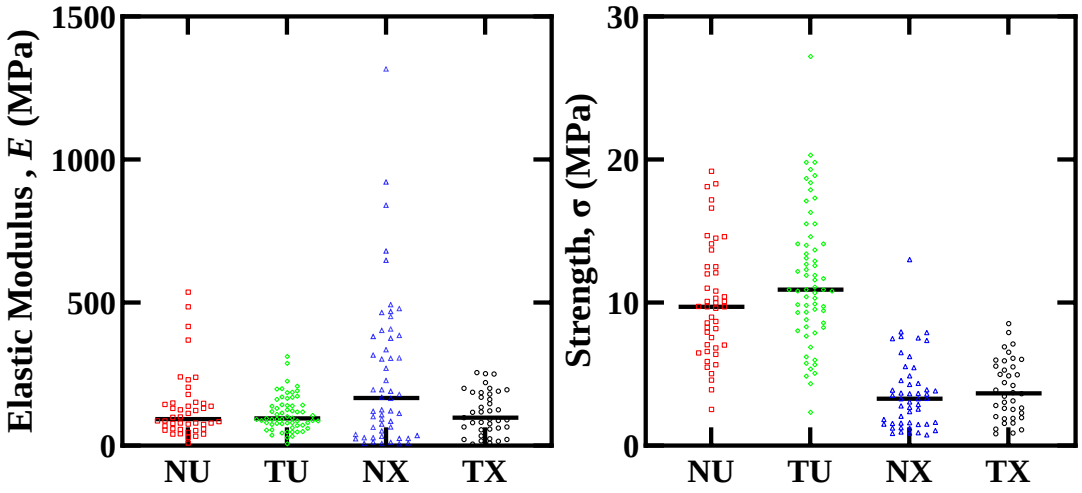

Figure 4.8: Elastic modulus and strength values for all four categories of electrospun fiber mats with a bar located at the average corresponding value.

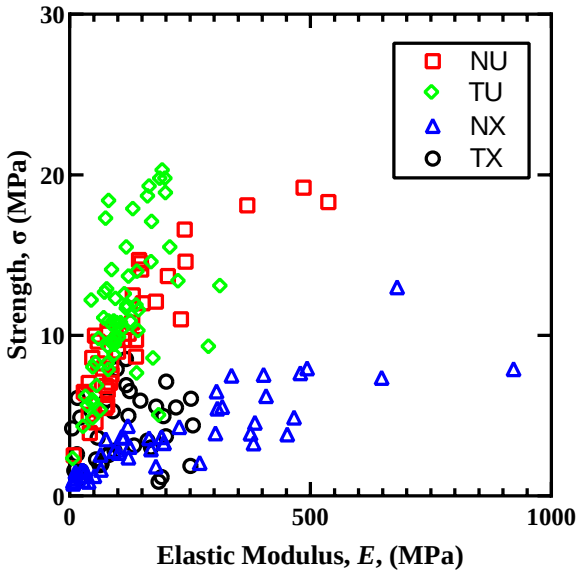

Figure 4.9: Strength as a function of elastic modulus for electrospinning study.

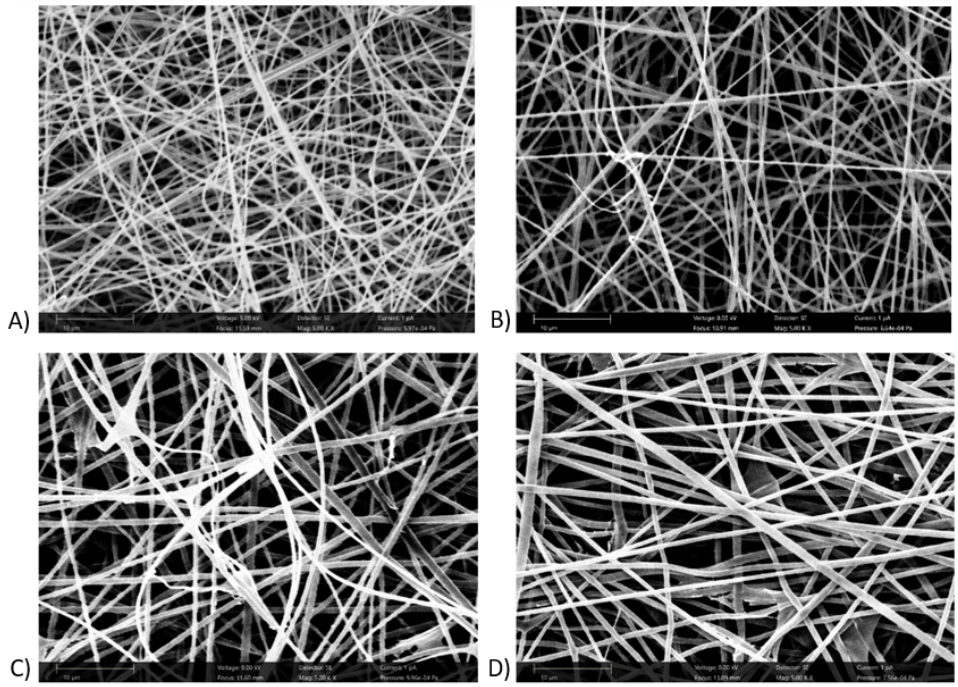

Figure 4.10: A) Not treated uncrosslinked (NU) B) Treated uncrosslinked (TU) C) Not treated crosslinked (NX) and D) Treated crosslinked (TX). The scale of each image is 10 μm.

4.4 Discussion

The second part of this project focused on the creation of biomimetic membranes (two types of gelatin polymer solutions: uncrosslinked and crosslinked) that can be used as a model system for a potential repair patch for a placental rupture site. As demonstrated in Figure 4.7, both sets of uncrosslinked fiber mats failed at much higher loads and displacements than the crosslinked fiber mats. Figure 4.8 shows that the elastic modulus values of each category are similar, with not treated crosslinked (NX) having the largest variability. Alternatively, there were distinct differences in strength values, such as both uncrosslinked mats having a much higher strength than the crosslinked mats. Figure 4.9 depicts an obvious trend in the data with strength as a function of elastic modulus. The NU, TU, and NX mat categories show that strength of the mats increased as elastic modulus increased, while the TX strength category did not increase notably as elastic modulus increased. However, Figure 4.9 does show a clear distinction of a greater strength in uncrosslinked mats compared to that of crosslinked. Overall, this data suggests that regardless of crosslinked or uncrosslinked, the not treated fiber mats showed the greatest values for both strength and elastic modulus. This indicates that the heat could have potentially degraded/melted the fibers, which made them weaker and less stiff. The SEM images showed that crosslinked fibers had a thicker diameter and larger porosity, which could indicate why the uncrosslinked fibers failed at greater loads and were stronger than the crosslinked mats.

This chapter discussed electrospinning nanofibers and how they were mechanically tested and imaged using SEM. These findings suggest that uncrosslinked fibers have a greater strength than crosslinked fibers, while there was no significant trend in the elastic modulus values among the different types of fibers. The next chapter will focus on the preparations and methods used to test fetal membranes in the same manner as the electrospun fibers, with the addition of a physiological stressor - collagenase concentration.

CHAPTER 5

FETAL MEMBRANE STUDY

5.1 Introduction

The overall goal of this experiment was to understand the force required for human fetal membranes to mechanically fail, in order to develop ways to prevent this from happening in the future. To do so, fetal membranes treated and untreated by collagenase enzymes were mechanically tested and analyzed in the same manner as the electrospun fiber mats. After mechanical testing was completed, the membranes were then analyzed using Fourier transform infrared spectroscopy (FTIR).

The FTIR machine analyzes the biological macromolecule components of materials [23]. A light is used to shine on a specimen as its intensity is measured by an infrared detector [23]. The Fourier transform is applied to this intensity and plotted as a function of wavelength value [23]. Components, such as proteins, lipids, nucleic acids, and carbohydrates, are able to be detected through a spectrum graph. Of these, the proteins and polypeptides, referred to as the Amide I and II bands, respectively, are analyzed most often [23], [39]. Amide I is typically the most intense absorption protein band while the Amide II band is much more complex [23]. The Amide I band is where collagen type I can be located. Therefore, the third part of this project focused on the mechanics of real fetal membranes and analyzed the effects of varying concentrations of degrading enzymes, such as collagenase, on these membranes.

5.2 Methods

Pregnant participants were consented as part of a larger pregnancy study. All protocols and processes were approved by the East Carolina University Institutional Review Board (IRB) and

followed standard code of ethics. All pregnant participants provided written informed consent. After delivery, human CA membranes were acquired from Vidant Medical Center and placed in a -80 °C freezer. When removed from the freezer the day prior to testing, samples were placed in the 0 °C fridge to thaw. Before testing began, a TESCA buffer was created to act as the control solution. The TESCA buffer was composed of TES buffer at 99.7 weight percent and calcium chloride (CaCl2) at 0.35 weight percent and was dissolved in distilled water and stirred. Once dissolved, pH strips were used to ensure the pH level of the TESCA solution was approximately 7.4. If the pH was initially too low, sodium hydroxide was added until there was a pH of 7.4. If the pH was too high, hydrochloric acid was added until a pH of 7.4 was obtained. Next, 24 mL of finalized TESCA buffer was placed into two centrifuge tubes. The remainder of the TESCA buffer was used as the control solution.

Collagenase at 0.036 weight percent was placed into one centrifuge tube of TESCA buffer to create the 45 U/mL collagenase concentration. Similarly, collagenase at 0.108 weight percent was placed into the second centrifuge tube of TESCA buffer to create the 135 U/mL collagenase concentration. The collagenase concentrations were selected based on a similar preliminary study. Both of these solutions were placed into the hot water bath at 37 °C until the collagenase was fully dissolved.

All fetal membrane preparation was conducted in a cell culture room under the biosafety cabinet. While the collagenase was dissolving in the TESCA buffer, the fetal membranes were removed from the fridge and placed onto a cutting board. The samples were straightened to be measured with a ruler and then placed with the chorion faced up and amnion side in contact with the cutting board. The chorion was scrapped/peeled off of the amnion and discarded into a biohazard waste bag. An example of the chorion versus the amnion is displayed in Figure 5.1.

A 3D printed 30 mm $\times$ 30 mm block was used to trace an appropriately sized cutout that was needed to fit across the cutout in the grips for mechanical testing. The number of slices from each sample varied due to inconsistency of membrane size. Once slices were cut from the membranes,

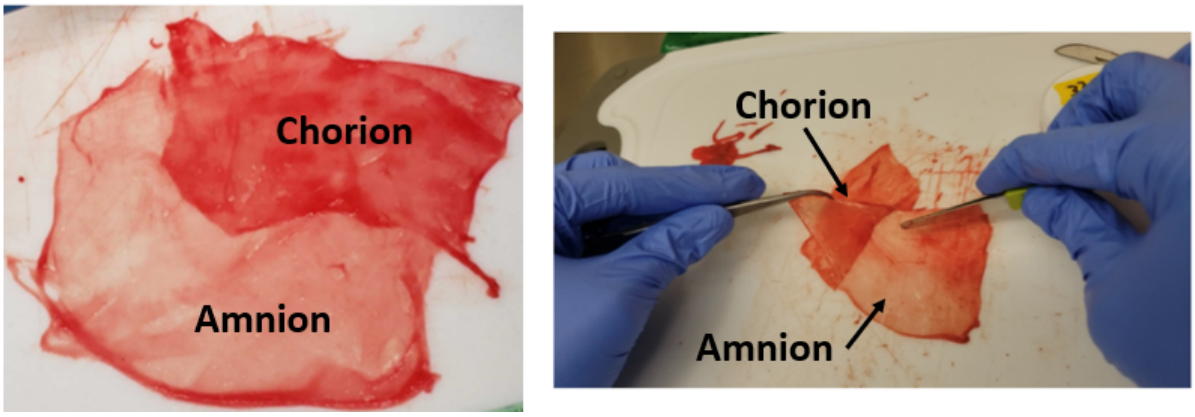

Figure 5.1: Fetal membrane sample showing the chorion and amnion being pulled apart.

they were placed in petri dishes filled with either a TECSA buffer solution serving as the control, a 45 U/mL collagenase concentration, or a 135 U/mL collagenase concentration. For example, if six slices were able to be obtained from a membrane, two slices were submerged in separate petri dishes filled with TESCA solution, two slices were submerged in separate petri dishes filled with 45 U/mL collagenase concentration solution, and the same for the 135 U/mL collagenase concentration solution. After all slices were submerged in either the control or a collagenase solution, they were immediately placed in the incubator set at 37 °C. Samples were incubated for 30 minutes or 60 minutes. When the respective incubation time was complete, each petri dish was removed and immediately placed in a Pyrex dish filled with ice to prevent further degradation from occurring. Next, the solution in each petri dish was removed with a pipette and replaced with phosphate buffered saline (PBS) solution until the sample was tested. Figure 5.2 shows the samples placed in ice immediately after being removed from the incubator and what the solution typically looked like after degradation occurred for each collagenase concentration.

Mechanical testing of the fetal membranes was conducted in the same manner as the electrospun fibers with an addition of polydimethylsiloxane (PDMS) slices placed between the grips to prevent the samples from slipping. The individual slices were held between the 3D printed grips and PDMS slices and placed onto the Zwick Roell machine. The same probe was lowered at a rate

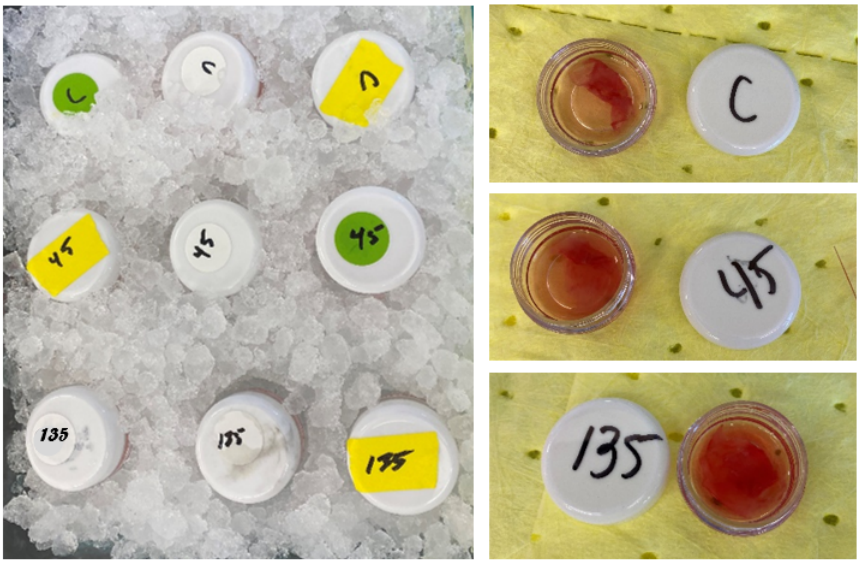

Figure 5.2: Samples placed in ice directly after incubation and visualization of a change in solution color after samples degraded in TESCA buffer and at 45 U/mL and 135 U/mL collagenase concentration solution.

of 0.5 mm/s until the samples fully failed. An example of a fully tested fetal membrane can be seen in Figure 5.3.

After mechanical testing was complete, the samples were placed back into their respective petri dishes with PBS solution until they were placed onto a sheet of aluminum to be analyzed using FTIR. A sample being tested on the FTIR machine can be seen in Figure 5.4. A mapping position of a 3×3 array was setup to take a total of nine points per sample. This means the FTIR probe contacted the sample in nine different locations and provided a spectrum line of the chemical makeup for each point. An example of an image with the nine scan points is shown in 5.5. Once each sample was tested, the median of the nine spectrum lines was extracted and combined on one graph per collagenase concentration and incubation time, making a total of six graphs: 3 solutions $\times$ 2 incubation times. From these six graphs, the median spectra line for each sample was extracted and placed on one final graph for easy comparison to each collagenase concentration group and incubation time.

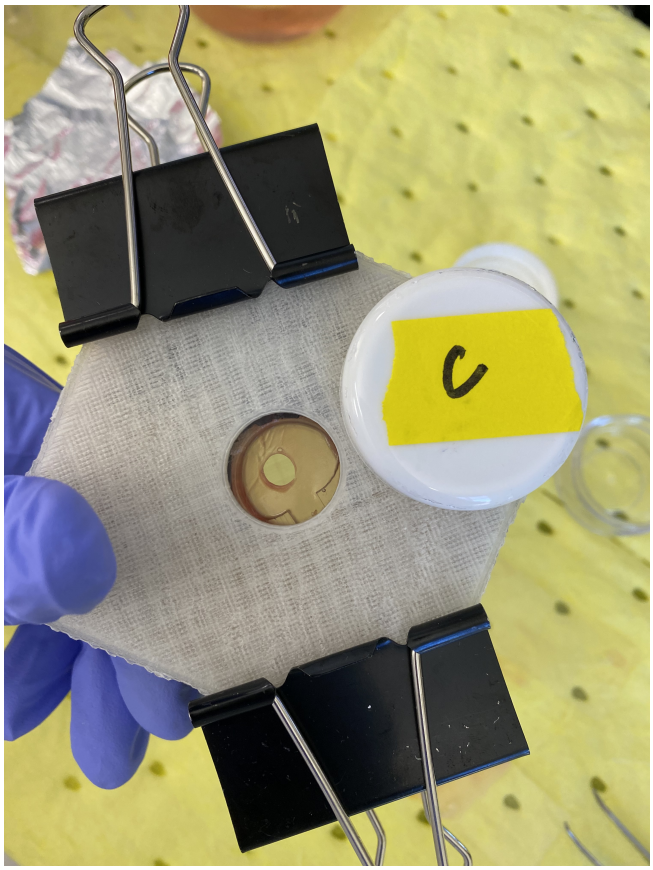

Figure 5.3: A fully punctured fetal membrane.

5.3 Results

The raw data for failure load as a function of displacement for fetal membranes can be seen in Figure 5.6. Control samples at both incubation times seemed to consistently fail between 6 and 8 mm, while the majority of the samples submerged in 45 U/mL and 135 U/mL collagenase concentrations failed between 4 and 6 mm. Loads up to approximately 11 N were obtained for the control samples, while loads stayed less than 5 N for the collagenase groups.

The results for the fetal membrane testing can be seen in Figure 5.7. The data shown in Figure 5.7 is displayed on the logarithmic scale. On the log scale, the elastic modulus for all concentration solutions and incubation times showed minimal variation from approximately 4 MPa to 9.5 MPa. The strength values varied between 0.3 to 3 MPa but had a stronger trend.

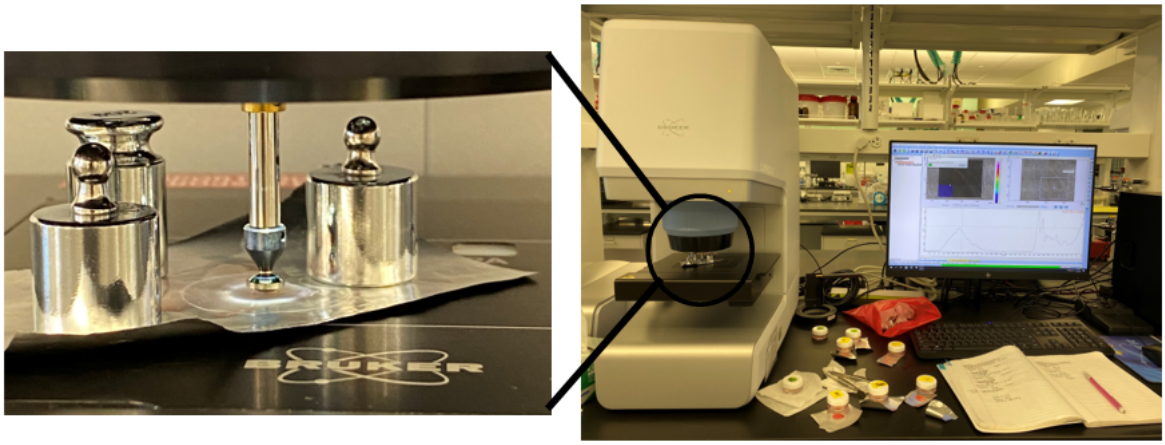

Figure 5.4: The Bruker FTIR spectroscopy machine testing a fetal membrane.

A graph displaying how the strength of the membranes changes as a function of elastic modulus can be seen in Figure 5.8 where strength values range from 0 MPa to $\sim$ 7 MPa and elastic modulus values range from 0 to 43 MPa. The FTIR results for the fetal membrane study can be seen in Figure 5.9. The cutoff wavenumbers ranged from 1800 to 800 due to this area being the fingerprint region and providing the most indicative chemical results within the peaks. The most significant peak for this project is the first peak, the Amide I band, as this indicates the level of collagen type I within the sample.

A linear regression model was used to analyze the elastic modulus and strength data (Table 5.1). The elastic modulus and strength data were originally skewed. Because a linear regression model assumes the data are normally distributed, a variable transformation was applied to the base-10 logarithmic scale for all elastic modulus and strength data. When discussing the significance of results, this was based on the p-value where a p-value ≤ 0.05 represents significant.

5.3.1 Results: Elastic Modulus

The only data that was significant in the elastic modulus model was the 135 U/mL collagenase concentration group. This model had an adjusted R^2 value of 0.025, which means 2.5% variance of elastic modulus was explained by collagenase concentration and incubation time.

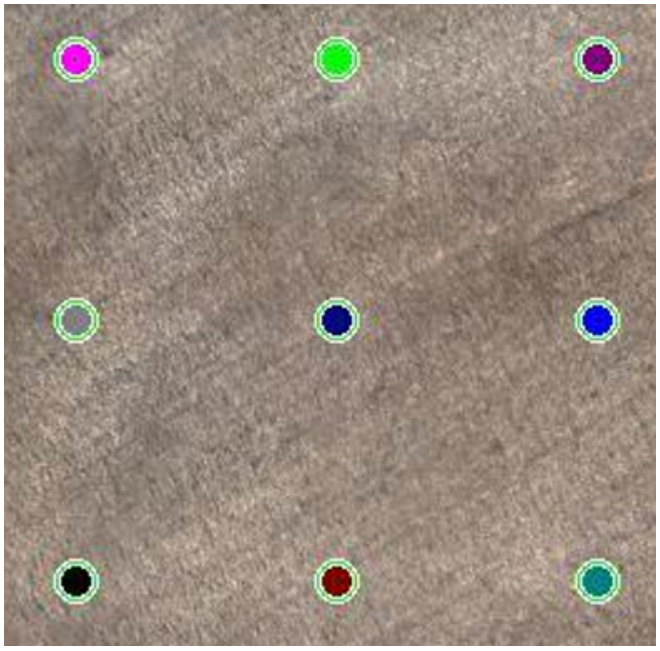

Figure 5.5: FTIR image of fetal membranes with the 3 $\times$ 3 array indicating the location of points measured. The colors on the points represent the corresponding color of the spectra line of the initial graph. The median of these lines was later extracted.

A significant difference was noted between the 135 U/mL collagenase concentration and the control group ($b = -0.253$, $p = 0.034$) while controlling incubation time. Alternatively, no significant differences were noticed between the 45 U/mL collagenase concentration and the control group ($b = -0.036$, $p = 0.693$) or the 30 minute and 60 minute incubation times ($b = -0.003$, $p = 0.256$). The average difference between the 135 U/mL collagenase concentration group and the control group in a base-10 logarithmic scale was -0.253, which is equivalent to 1.79 MPa.

5.3.2 Results: Strength

This entire regression model was significant with an adjusted R^2 value of 0.246, which means 24.6% variance of strength was explained by incubation time and collagenase concentration. There was a significant difference between 45 U/mL collagenase and control group ($b = -0.249$, $p = 0.002$) and also between 135 U/mL collagenase with control group ($b = -.524$, $p =< 0.001$) while

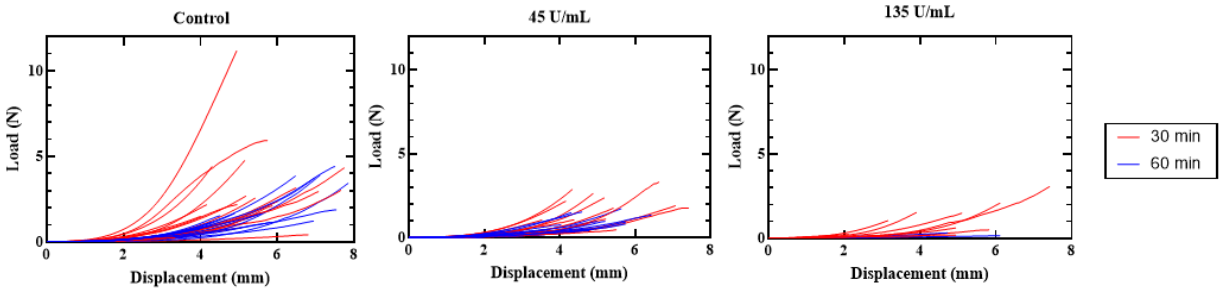

Figure 5.6: The failure load as a function of displacement curves for fetal membranes at each collagenase concentration.

Table 5.1: Statistical results for elastic modulus and strength for fetal membrane study where the bold values are significant values.

		Elastic Modulus	Strength
	R^2	0.025	0.246
30 min vs. 60 min	Unstandardized b	-0.003	-0.007
	Standardized Coefficient β	-0.125	-0.259
	p-value	0.256	**0.007**
45 U/mL vs. Control	Unstandardized b	-0.036	-0.249
	Standardized Coefficient β	-0.046	-0.309
	p-value	0.693	**0.002**
135 U/mL vs. Control	Unstandardized b	-0.253	-0.524
	Standardized Coefficient β	-0.250	-0.513
	p-value	**0.034**	**<0.001**

the incubation time was controlled. There was also a significant difference between the 30 minute and 60 minute incubation times ($b = -0.007$, $p = 0.007$).

The average differences between the two different incubation times in a base-10 logarithmic strength was -0.007 which is equal to 1.02 MPa. The average differences between 45 U/mL collagenase and control group in base-10 logarithmic scale was -0.249, which is equivalent to 1.77 MPa. The average differences between 135 U/mL collagenase and control group in base-10 logarithmic scale was -0.524, which is equivalent to 3.34 MPa.

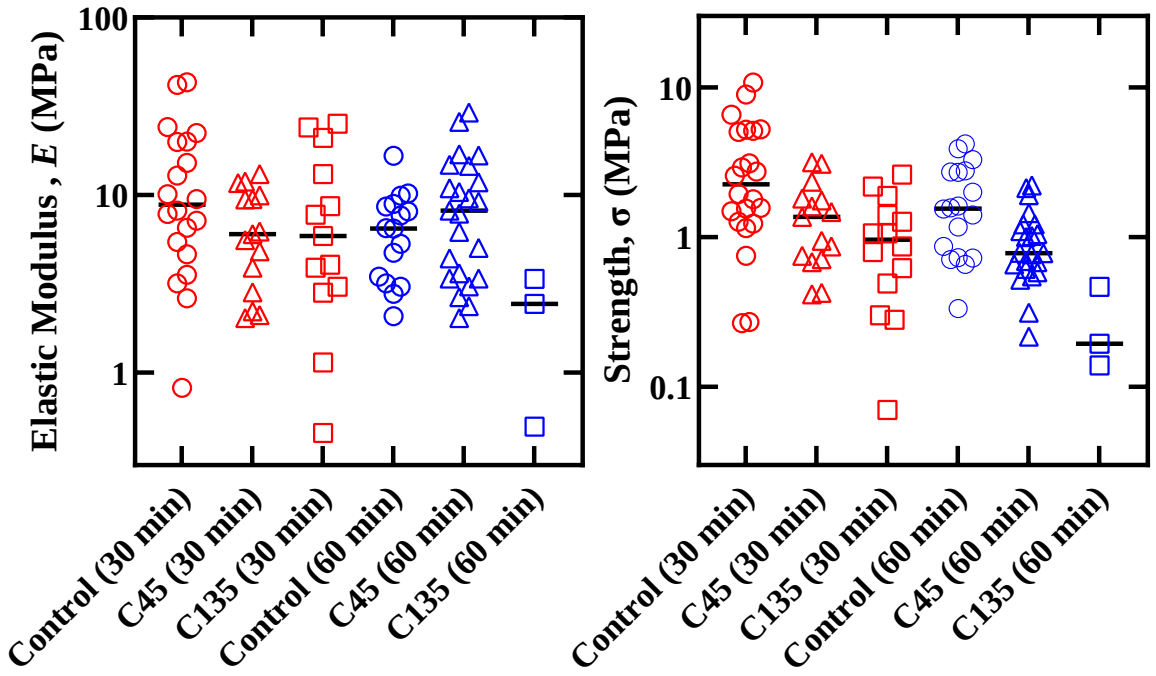

Figure 5.7: The elastic modulus and strength results for fetal membrane mechanical testing.

5.4 Discussion

The third part of this project focused on the mechanics of real fetal membranes and analyzed the effects of varying concentrations of collagenase on these membranes. Regarding the FTIR results, there was a relatively consistent amount of collagen type I detected within the Amide I band throughout the varying concentration solutions and incubation times.

Interestingly, there is not a significant trend within the elastic modulus values for fetal membranes, but there is a strong relationship between the strength of the membranes and the respective solution and incubation time. It is evident that as collagenase concentration increases, the strength of the membranes decreases for both incubation times. The adjusted R^2 factors for both elastic modulus and strength indicate that other factors which are not within this model could explain

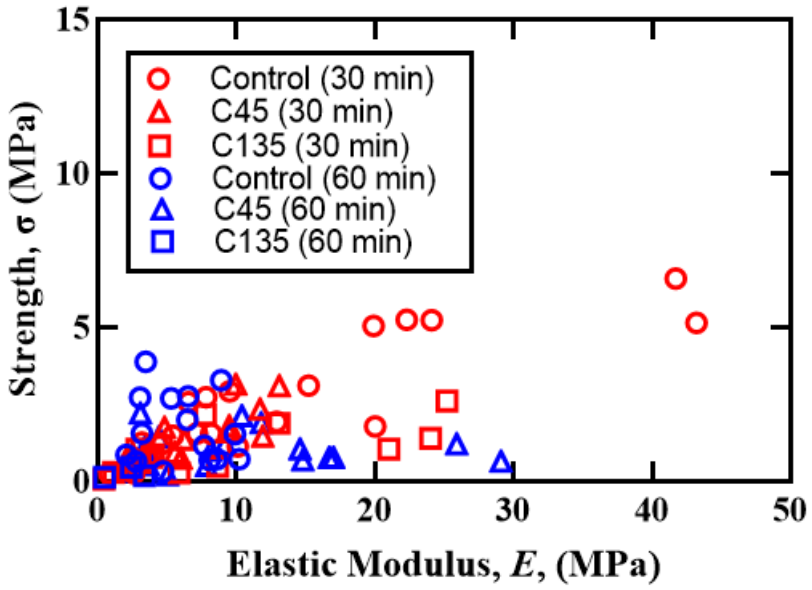

Figure 5.8: Strength as a function of elastic modulus for the fetal membranes at varying collagenase concentration levels and incubation times.

the variance of elastic modulus and strength. The statistical analysis suggests that incubation time did not significantly impact the elastic modulus of the samples, which is consistent with the data displayed in Figure 5.7. This could be an indication that temperature does not have a strong effect on the elastic modulus of fetal CA membranes. Alternatively, the strength of a material and temperature have a much stronger trend. The data analysis implies that more membrane degradation occurred with a higher collagenase concentration, resulting in a lower elastic modulus and strength.

When fetal membranes were submerged in a 45 U/mL collagenase concentration, there was no significant change in elastic modulus but there was a decrease in strength by 1.77 MPa. Similarly, when the fetal membranes were incubated for 60 minutes rather than 30 minutes, the elastic modulus did not vary significantly, but the strength decreased 1.02 MPa. When fetal membranes were submerged in a 135 U/mL collagenase concentration, the elastic modulus and strength of the membranes decreased by 1.79 and 3.34 MPa, respectively.

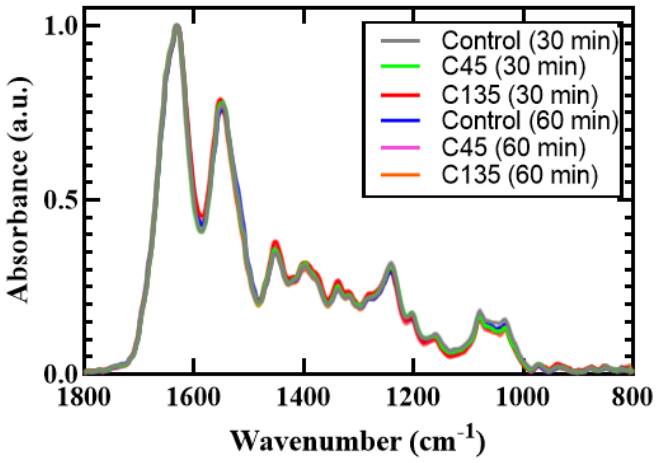

Figure 5.9: FTIR results for the fetal membrane study.

This chapter focused on the mechanical testing of fetal membranes and how they were analyzed using FTIR spectroscopy. The data suggests that the strength of fetal membranes decreases as collagenase concentration increases and as incubation time increases. Additionally, the elastic modulus of the membranes decreased only at the greater collagenase concentration. Therefore, this indicates that as collagenase enzymes build up throughout pregnancy and stay within the woman incubating at body temperature, the strength and elastic modulus of the fetal CA membranes will decrease and could lead to PPROM. The next chapter will consider all of the previous results and make conclusions based on testing.

CHAPTER 6

CONCLUSION AND FUTURE WORK

The need for a prevention of preterm birth is evident. This project included several aspects related to pregnancy research and treatment for understanding mechanisms related to preterm birth, including conducting mechanical testing on a nanoscale, using the process of electrospinning to create artificial biomimetic membrane patches, and mechanically testing human fetal membranes to obtain the elastic modulus and strength.

Nanoindentation testing was conducted on manufactured Matrigen® hydrogels and polyacrylamide hydrogels that were fabricated in the lab. This portion of the project served as a method of obtaining calibration factors and techniques on a small scale and on materials measuring in the kPa range. This testing showed that the elastic modulus was consistently lower than anticipated for both Matrigen® and polyacrylamide gels. This indicates that there is still testing that needs to be conducted in order to be confident in nanoindentation in the kPa range, especially for biological materials.

Electrospinning was conducted as an approach of creating a potential patch to stitch and repair the placental membranes if preterm pre-labor rupture of membranes occurs. Four different categories of nanofiber mats were fabricated, including not heat treated crosslinked (NX), not heat treated uncrosslinked (NU), heat treated crosslinked (TX), and heat treated uncrosslinked (TU). The mechanical testing of these mats indicated that there were minimal differences in elastic modulus among the mats; however, both uncrosslinked fiber mats had much greater strengths than the crosslinked mats. This data serves as a pathway to the future of a potential artificial biomimetic membrane patch in preventing preterm birth.

The last portion of this project included the testing of human fetal membranes. The membranes were separated into three different groups including a control group, 45 U/mL collagenase concentration, and 135 U/mL collagenase concentration. As collagenase is a catabolic protein in the human body, it is important to understand how it could impact pregnancy. When collagenase reached the highest concentration tested, the elastic modulus decreased. There was also a decrease in strength as incubation times and collagenase concentration increased. Overall, this testing suggests that if the woman obtains collagenase buildup, PPROM is more likely to occur, which could potentially lead to preterm birth.

Although this project resulted in many results, there is still critical research required related to pregnancy research. Moving forward, a logical next step is to mechanically test the electrospun fiber mats after being submerged in the same control and collagenase concentrations as the fetal membranes to see how they respond relative to the human fetal membranes. More development and eventually collaboration and communication are needed between researchers and obstetricians on how to feasibly implement a potential patch on the placenta to repair ruptured membranes. When discussing the implementation of a potential patch, the financial aspect is also an important discussion.

Overall, there was not a distinct trend in elastic modulus regarding electrospun fibers, but there was a significant decrease in elastic modulus values for fetal membranes at higher collagenase concentrations. There was a significant difference in strength values of electrospun fibers depending on the fiber mat crosslinking with NU and TU being stronger. There was also a significant decrease in strength for fetal membranes at both collagenase concentrations and incubation times. Overall, it appears that NU and TU fiber mats could potentially be used as patches for PPROM. Further research will also need to examine how to apply a potential patch.

REFERENCES

[1] March of Dimes. *What is Full Term?* (September 2018). https://www.marchofdimes.org/pregnancy/what-is-full-term.aspx.

[2] Merriam-Webster. *Dictionary by Merriam-Webster: America's most-trusted online dictionary* (n.d.). https://www.merriam-webster.com/.

[3] March of Dimes. *Preterm Labor and Premature Birth: Are You at Risk?* (March 2018). https://www.marchofdimes.org/complications/preterm-labor-and-premature-birth-are-you-at-risk.aspx.

[4] Mercer, Brian. "Preterm Premature Rupture of the Membranes" *Obstetrics & Gynecology* 101 (1): 178-193, 2003. https://doi.org/10.1016/S0029-7844(02)02366-9.

[5] March of Dimes. *Special Care Nursery Admissions* (2011). https://www.oakbendmedcenter.org/wp-content/uploads/2018/05/nicu_summary_final.pdf

[6] Calvin, Steven and Michelle Oyen. "Microstructure and Mechanics of the Chorioamnion Membrane with an Emphasis on Fracture Properties" *Annals of the New York Academy of Sciences* 1101: 166–85, 2007. https://doi.org/10.1196/annals.1389.009.

[7] Mayo Clinic. *Preterm Labor*. (n.d.). https://www.mayoclinic.org/diseases-conditions/preterm-labor/diagnosis-treatment/drc-20376848.

[8] Mayo Clinic. *Fetal Fibronectin Test*. (n.d.). https://www.mayoclinic.org/tests-procedures/fetal-fibronectin/about/pac-20384676#: :text=Fetal%20fibronectin%20is%20a%20protein,into%20secretions%20near%20your%20cervix.

[9] Mother To Baby. *Critical Periods of Development* (December 1, 2019). https://mothertobaby.org/fact-sheets/critical-periods-development/.

[10] Fuentes, Armando. KidsHealth. *Treatments to Prevent Premature Birth* (October, 2018). https://kidshealth.org/en/parents/treatments-prevent-premature-birth.html.

[11] Mayo Clinic. *Premature birth*. (April 14, 2021). https://www.mayoclinic.org/diseases-conditions/premature-birth/symptoms-causes/syc-20376730.

[12] Chua, Wesley and Michelle Oyen. "Viscoelastic Properties of Membranes Measured by Spherical Indentation" *Cellular and Molecular Bioengineering* 2: 49-56, 2009. https://doi.org/10.1007/s12195-009-0049-7.

[13] Wheeler, Mackenzie and Michelle Oyen. "Bioengineering Approaches for Placental Research" *Annals of Biomedical Engineering* 49 (8): 1805-1818, 2021. https://doi.org/10.1007/s10439-020-02714-7.

[14] Chua, Wesley and Michelle Oyen. "Do We Know the Strength of the Chorioamnion? A Critical Review and Analysis" *European Journal of Obstetrics, Gynecology, and Reproductive Biology* 144 (1): S128-33, 2009. https://doi.org/10.1016/j.ejogrb.2009.02.029.

[15] GCForsyth. Wikimedia Commons. *Fetal Membranes* (September 25, 2019). https://commons.wikimedia.org/wiki/File:Fetal_membrane.jpg.

[16] Bourne, Gordon. The Human Amnion and Chorion. Aylesbury, U.K., 1962, *Lloyd-Luke (Medical Books Limited) LTD.*.

[17] House, Michael, David Kaplan, and Simona Socrate. "Relationships between Mechanical Properties and Extracellular Matrix Constituents of the Cervical Stroma during Pregnancy" *Seminars in Perinatology* 33 (5): 300-307, 2009. https://doi.org/10.1097/01.AOG.0000284624.23598.7c.

[18] Healthline. *Top 6 Benefits of Taking Collagen Supplements* (February 19, 2020). https://www.healthline.com/nutrition/collagen-benefits.

[19] BruceBlaus. Wikimedia Commons. *Cervical Cerclage* (September 22, 2016). https://commons.wikimedia.org/wiki/File:Cervical_Cerclage.png.

[20] SMART Servier Medical Art. Wikimedia Commons. *Tendon anatomy - Tendon Epimysium Fascicle Fiber Fibril etc – Smart-Servier (cropped)* (September 29, 2019). https://commons.wikimedia.org/wiki/File:Tendon_anatomy_-_Tendon_Epimysium_Fascicle_Fiber_Fibril_etc_–_Smart-Servier_(cropped).jpg.

[21] Parry, Samuel and Jerome Strauss. "Premature Rupture of the Fetal Membranes" *The New England Journal of Medicine* 338: 663-670, 1998. https://doi.org/10.1056/NEJM199803053381006.

[22] Bhagwat, Prashant and Padma Dandge. "Collagen and Collagenolytic Proteases: A Review" *Biocatalysis and Agricultural Biotechnology*. 15, 2018. https://doi.org/10.1016/j.bcab.2018.05.005.

[23] Jabs, Andreas. "Determination of Secondary Structure in Proteins by Fourier Transform Infrared Spectroscopy (FTIR)" *Jena Library of Biological Macromolecules* (n.d.). http://jenalib.leibniz-fli.de/ImgLibDoc/ftir/IMAGE_FTIR.html.

[24] Shapiro, Jenna and Michelle Oyen. "Hydrogel Composite Materials for Tissue Engineering Scaffolds" *The Journal of The Minerals, Metals & Materials Society* 65 (4), 2013. https://doi.org/10.1007/s11837-013-0575-6.

[25] Law, Jia Xian, Ling Ling Liau, Aminuddin Saim, and Ying Yang. "Electrospun Collagen Nanofibers and Their Applications in Skin Tissue Engineering" *Tissue Engineering and Regenerative Medicine* 14: 699-718, 2017. https://doi.org/10.1007/s13770-017-0075-9.

[26] Qin, Xiao-Hong and Shan-Yuan Wang. "Filtration Properties of Electrospinning Nanofibers" *Journal of Applied Polymer Science* 102 (2): 1285-1290, 2006. https://doi.org/10.1002/app.24361.

[27] Subbiah, Thandavamoorthy, G. S. Bhat, R. W. Tock, S. Parameswaran, and S. S. Ramkumar. "Electrospinning of Nanofibers." *Journal of Applied Polymer Science* 96 (2): 557-569, 2005. https://doi.org/10.1002/app.21481.

[28] Wang, Xianfeng, Bin Ding, and Bingyun Li. "Biomimetic Electrospun Nanofibrous Structures for Tissue Engineering" *Materials Today* 16 (6): 229-241, 2013. https://doi.org/10.1016/j.mattod.2013.06.005.

[29] Collins, George, John Federici, Yuki Imura, and Luiz H. Catalani. "Charge Generation, Charge Transport, and Residual Charge in the Electrospinning of Polymers: A Review of Issues and Complications." *Journal of Applied Physics* 111:044701, 2012. https://doi.org/10.1063/1.3682464.

[30] Sundaray, Bibekananda, V. Subramanian, and T. S. Natarajan. "Electrospinning of Continuous Aligned Polymer Fibers." *Applied Physics Letters* 84: 1222, 2004. https://doi.org/10.1063/1.1647685.

[31] Huang, Liwei, Nhu-Ngoc Bui, Seetha Manickam, and Jeffrey McCutcheon. "Controlling Electrospun Nanofiber Morphology and Mechanical Properties Using Humidity" *Journal of Polymer Science Part B: Polymer Physics* 49 (24): 1734-1744, 2011. https://doi.org/10.1002/polb.22371.

[32] Shayegan, Marjan, Naghmeh Rezaei, Norman Lam, Tuba Altindal, Andrew Wieczorek, and Nancy Forde. "Probing Multiscale Mechanics of Collagen with Optical Tweezers" *Proceedings of SPIE - The International Society for Optical Engineering (Proceedings of SPIE)* 8810, 2013. https://doi.org/10.1117/12.2027258.

[33] Oyen, Michelle. "Nanoindentation of Hydrated Materials and Tissues" *Current Opinion in Solid State and Materials Science* 19 (6): 317-323, 2015. https://doi.org/10.1016/j.cossms.2015.03.001.

[34] Pharr, George. "A Brief History of Nanoindentation - and a Little More" *Materials Science and Engineering* (2021). https://materials.engineering.unt.edu/seminars/2021/brief-history-nanoindentation-and-little-more.

[35] Tonsomboon, Khaow, Annabel Butcher, and Michelle Oyen. "Strong and Tough Nanofibrous Hydrogel Composites Based on Biomimetic Principles" 72 (1): 220-227, 2017. *Materials Science & Engineering*. https://doi.org/10.1016/j.msec.2016.11.025.

[36] Repanas, Alexandros, Sofia Andriopoulou, and Birgit Glasmacher. "The Significance of Electrospinning and a Method to Create Fibrous Scaffolds for Biomedical Engineering and Drug Delivery Applications" *Journal of Drug Delivery Science and Technology*. 31: 137-146, 2016. https://doi.org/10.1016/j.jddst.2015.12.007.

[37] Ludwick, Jacob and Michelle Oyen. "Towards the Development of a Cartilage-like Nanofiber-Hydrogel Composite" *Materials Research Society Advances* 5 (33-34): 1783-1790, 2020. https://doi.org/10.1142/s0219519411004848.

[38] Oyen, Michelle, Robert Cook, and Steven Calvin. "Mechanical Failure of Human Fetal Membrane Tissues" *Journal of Materials Science, Materials in Medicine* 15 (6): 651-658, 2004. https://doi.org/10.1023/b:jmsm.0000030205.62668.90.

[39] Gallagher, Wallen. "FTIR Analysis of Protein Structure" *Course Manual Chem* 455, 2009. https://www.chem.uwec.edu/chem455_S05/Pages/Manuals/FTIR_of_proteins.pdf.